Popova, E.E.; Yool, A.; Aksenov, Y.; Coward, A.C.. 2013 Role of advection in Arctic Ocean lower trophic dynamics: a modelling perspective. *Journal of Geophysical Research: Oceans*, 118 (3). 1571-1586. 10.1002/jgrc.20126

Popova, E.E.; Yool, A.; Aksenov, Y.; Coward, A.C.. 2013 Role of advection in Arctic Ocean lower trophic dynamics: a modelling perspective. *Journal of Geophysical Research: Oceans*, 118 (3). 1571-1586. 10.1002/jgrc.20126

Role of advection in Arctic Ocean lower trophic dynamics: A modeling perspective

E. E. Popova,[1] A. Yool,[1] Y. Aksenov,[1] and A. C. Coward[1]

Received 3 August 2012; revised 7 February 2013; accepted 12 February 2013; published 28 March 2013.

[1] The Arctic Ocean (AO) is an oligotrophic system with a pronounced subsurface Chl-a maximum dominating productivity over the majority of the basin. Strong haline stratification of the AO and substantial ice cover suppress vertical mixing and restrict the vertical supply of nutrients to the photic zone. In such a vertically stratified oligotrophic system, the horizontal supply of nutrients by advection plays an important role in sustaining primary production. In this paper, we attempt to characterize the role of nutrient advection in the maintenance of the subsurface Chl-a maximum, using timescales to determine the connectivity between the photic zone of the deep AO, nutrient-rich Pacific and Atlantic inflow waters, and bottom waters of the wide continental shelves of the AO. Our study uses output from a general circulation model, Nucleus for European Modeling of the Ocean, coupled to a model of ocean biogeochemistry, Model of Ecosystem Dynamics, carbon Utilization, Sequestration, and Acidification. A Lagrangian particle tracking approach is used to back-track water from where it forms subsurface Chl-a maxima to the points of entry into the AO and to analyze nutrient transformation along the route. Our experiments show that advective timescales linking subsurface layers of the central AO with the nutrient-rich Pacific and Atlantic waters do not exceed 15–20 years and that the advective supply of shelf nutrients to the deep AO occurs on the timescale of about 5 years. We show substantial role of the continental shelf pump in sustaining up to 20% of total AO primary production.

Citation: Popova, E. E., A. Yool, Y. Aksenov, and A. C. Coward (2013), Role of advection in Arctic Ocean lower trophic dynamics: A modeling perspective, *J. Geophys. Res. Oceans*, *118*, 1571–1586, doi:10.1002/jgrc.20126.

1. Introduction

[2] The upper Arctic Ocean (AO) is strongly stratified [e.g., *Aagaard et al*., 1981 with a low salinity upper mixed layer (UML) overlying a strong halocline commonly found between 50 and 250 m [*Rudels et al*., 1996]. In summer, melting of sea ice creates a surface layer of still lower salinity on top of the existing UML.

[3] Another prominent feature of the AO is its continental shelf regions which have significant differences with other shelf regions of the World Ocean. They are very wide (Figure 1), they are influenced by the process of seasonal sea-ice formation and melting, and they experience significant riverine input that enforces strong water column stratification [e.g., *Anderson et al*., 2010]. In such a strongly stratified water column, primary production in the UML of the AO is limited by nutrients [*Tremblay and Gagnon*, 2009; *Martin et al*., 2010; *Wassmann*, 2011; *Popova et al*., 2010]. Exceptions occur in areas such as the Atlantic inflow with its characteristic deep winter mixing (Norwegian Sea), the Southern Chukchi Sea with its strong advective supply of nutrients from the Pacific, polynyas [e.g., *Tremblay et al*., 2011], and areas of strong shelf break upwelling [*Williams & Carmack*, 2008; *Tremblay et al*., 2011].

[4] Strong vertical stratification and low nutrient concentrations in the UML allow for the development of subsurface Chl-a maxima (SCM), which are formed when phytoplankton grow below the UML as a compromise between light availability from above and nutrient availability from below [e.g., *Martin et al*., 2010]. Indeed, recent observational and modeling studies find that SCM is a ubiquitous feature of the AO [e.g., *Hill & Cota*, 2005; *Martin et al*., 2010; *McLaughlin & Carmack*, 2010; *Popova et al*., 2010]. Furthermore, *Martin et al*. [2010] have suggested that the SCM fraction of total primary production may be an order of magnitude higher than that typically observed in the oligotrophic low latitudes. This increased importance of the SCM in the AO stems from the very thin and stable AO UML and the sharp AO nutricline, which allow formation of the SCM at shallower depths and earlier in the season than in other oligotrophic areas [*Martin et al*., 2010]. In addition, *Martin et al*. [2010] found that the SCM in the northern Baffin Bay was dominated by large diatom phytoplankton leading to the co-occurrence of a subsurface biomass maxima with the SCM. Analysis of the recently published AO Chl-a

[1]National Oceanography Center, University of Southampton Waterfront Campus, Southampton, Hampshire, UK.

Corresponding author: E. E. Popova, National Oceanography Center, University of Southampton Waterfront Campus, Empress Dock, Southampton, Hampshire, SO14 3ZH, UK. (E.Popova@noc.ac.uk)

2169-9275/13/10.1002/jgrc.20126

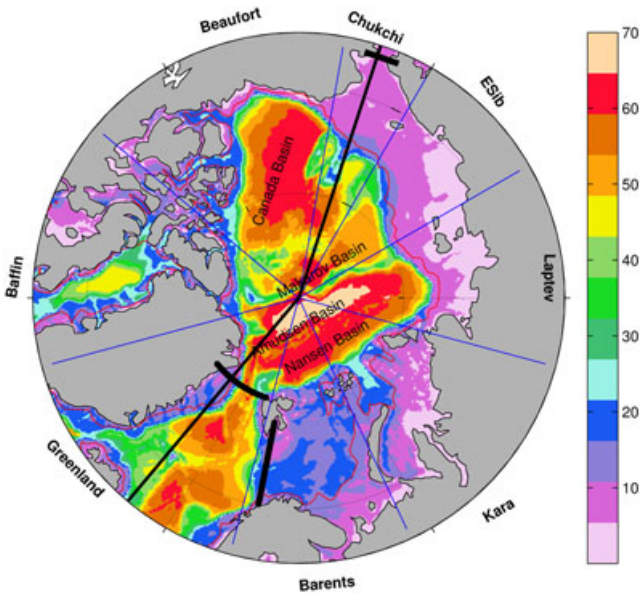

Figure 1. AO bottom topography (m). Thick black lines indicate three geographical interception sections used in Lagrangian analysis. Location of the cross section from Figure 4 is shown as a thin black line.

and productivity database [*Arrigo et al*., 2011] finds that, on average, 43% of total water column Chl-a in observed locations occurs below the depth of 20 m (see Methods for details of this estimate). Meanwhile, a modeling study by *Popova et al*. [2010] has suggested that 46% of AO primary production occurs below the UML. Melting of AO sea ice and expansion of the seasonally ice-free region under future climate change may further increase the significance of the SCM [*Martin et al*., 2010; *McLaughlin & Carmack*, 2010]. Thus, it is crucial to understand which physical processes control the nutrient content of the upper part of the halocline in the AO from the base of the summer UML to the bottom of the photic zone (O(100 m)) where short-wave radiation is still sufficient for nutrient utilization by phytoplankton. In a strongly stratified system where vertical turbulent fluxes of nutrients are restricted, advective regulation of ecosystems dynamics comes to the forefront. Advective processes connect the AO with nutrient-rich waters from the northern North Pacific and Atlantic Oceans and the deep AO with the adjacent shelf areas where substantial transformation of the biogeochemical characteristics occurs [e.g., *Jones & Anderson*, 1986]. In addition, shelf regions in the Chukchi Sea have a strong and continuous supply of nutrients from the Pacific Ocean through the shallow Bering Strait. However, in common with other shelf regions, those in the AO are comparatively productive relative to deep ocean regions, although levels of shelf productivity vary substantially around the AO dependent on their proximity to the inflow of high nutrient Pacific or Atlantic waters [e.g., *Carmack & Wassmann*, 2006].

[5] *Jones & Anderson* [1986] proposed a mechanism for the shelf origin of the biogeochemical properties of the upper halocline. During sea-ice formation on the outer shelves, brine production creates saline bottom water. Overlying fresh riverine water prevents vertical mixing with this denser bottom water and prevents re-entrainment of remineralized nutrients into the photic layer. Thus, all particulate organic matter reaching the seafloor on the shelves is remineralized there, but the constituent nutrients are prevented from returning to the photic zone locally and instead are advected horizontally into the deep AO under the UML. *Jones & Anderson* [1986] argued that while Bering Sea and northern North Atlantic can be recognized as sources of halocline waters, the biogeochemical composition of the water masses from these areas undergoes substantial changes under the influence of the Arctic shelves. Subsequently, *Anderson et al*. [2010] showed that the continental shelf pump in the East Siberian and Chukchi seas results in an excess of carbon and nutrients in subsurface waters of Canadian Basin; *Nitishinsky et al*. [2007] and *Dmitrenko et al*. [2011] showed enhanced near-bottom nutrient concentrations in the Laptev Sea over midshelf to the shelf break region (depth range of 30–100 m); and *Alkire et al*. [2010], on the basis of NO ($NO = 9 \times [NO_3^-] + [O_2]$) measurements, deduced a direct influence from the Siberian shelves in the halocline layer of the Makarov basin.

[6] In this study, we attempt to analyze AO ecosystems from an advective perspective. Combining output from a high-resolution, global-scale model that includes ecosystem dynamics with Lagrangian particle tracking, we investigate the connectivity between various AO regions and calculate timescales associated with the impact of advection on AO ecosystems. We follow the pathways of water masses that track the origins of the upper nutricline waters, which in turn provide nutrients for phytoplankton to utilize during the productive summer season. Our analysis presents a quantitative description of the role of advection in AO ecosystem dynamics. A more traditional, Eulerian analysis of the physical factors controlling AO primary production within the framework of the same model is described in *Popova et al*. [2010].

2. Methods

2.1. Coupled Physical and Biological Model

[7] The global Nucleus for European Modeling of the Ocean (NEMO) configurations of 1/4° resolution have been successfully used in various studies of the North Atlantic and of the AO [e.g., *Lique et al*., 2010; *Grist et al*., 2010; *Marsh et al*., 2010; *Popova et al*., 2010; *Tsubouchi et al*., 2012]. The model's performance has been assessed in the Arctic Ocean Model Intercomparison Project [AOMIP; *Proshutinsky et al*., 2011], and a comparison of model results with observations is given in section 3. NEMO model is comprised of an ocean general circulation model (OGCM), OPA [*Madec*, 2008], coupled with the Louvain-la-Neuve Ice Model v2, LIM2 [*Timmermann et al*., 2005]. The version of NEMO used here is v3.2 and has a horizontal resolution of 1/4° and a vertical resolution of 64 levels with 14 levels in the top 100 m achieving resolution of 5 m near the surface and ~10 m at 100 m. NEMO is forced at the surface using DFS4.1 fields developed by the European DRAKKAR collaboration [*DRAKKAR Group*, 2007]. This combines the CORE dataset [*Large & Yeager*, 2004], from which precipitation and downward short- and long-wave radiation are extract, with the ERA40 reanalysis, from which 10 m wind and 2 m air temperature and humidity are extracted. The frequency of DFS4.1 is monthly for precipitation, daily for radiation and 6 hourly for turbulent variables.

Further details of the run used in this study can be found in *Popova et al*. [2010]. In addition, a 1° run is used for numerical experiments because of the prohibitive computational expense of the 1/4° resolution. This run is identical to that of *Yool et al*. [2011], with the exception that nutrient relaxation is inactivated.

[8] Biogeochemistry in NEMO is represented by the plankton ecosystem model Model of Ecosystem Dynamics, carbon Utilization, Sequestration, and Acidification [MEDUSA; *Yool et al*., 2011]. This is a size-based, intermediate complexity model that divides the plankton community into "small" and "large" portions and which resolves the elemental cycles of nitrogen, silicon, and iron. The "small" portion of the ecosystem is intended to represent the microbial loop of picophytoplankton and microzooplankton, while the "large" portion covers microphytoplankton (specifically diatoms) and mesozooplankton. The intention of MEDUSA is to separately represent small, fast-growing phytoplankton that are kept in check by similarly fast-growing protistan zooplankton, and large, slower-growing phytoplankton that are able to temporarily escape the control of slower-growing metazoan zooplankton. The nonliving particulate detritus pool is similarly split between small, slow-sinking particles that are simulated explicitly, and large, fast-sinking particles that are represented only implicitly. See *Yool et al*. [2011] for a full description of MEDUSA.

[9] The simulation of NEMO used here was originally performed to produce a high-resolution, global-scale hindcast of marine biogeochemistry during the past two decades. An initial physics-only spin-up simulated the period 1978 to 1987 (10 years). The biogeochemistry was then coupled and MEDUSA was run for the period 1988 to 2007 (20 years). An analysis of the Arctic region in the resulting simulation has previously been published by *Popova et al*. [2010].

2.2. Lagrangian Analysis

[10] We use an off-line mass preserving Lagrangian scheme, ARIANE (http://stockage.univ-brest.fr/~grima/Ariane/). A description of the algorithm is given by *Doos* [1995] and *Blanke & Raynaud* [1997]. Lagrangian diagnoses are derived from the monthly mean velocity field of the high-resolution global model described in the previous section. In this approach, the main ocean circulation patterns (and associated timescales) are tracked by numerous point particles that are "released" into the model's flow field. Along its trajectory, a given particle will record changing properties (salinity, temperature, and biogeochemical characteristics), as given by the local Eulerian fields of the ocean model. The Lagrangian scheme does not consider turbulent mixing in the trajectory calculations; however, as the ocean model parameterizes such mixing, its signature is present in the physical and biogeochemical properties along the computed trajectories.

[11] Such a Lagrangian analysis has been carried out successfully in a variety of global and regional ocean circulation studies using OGCM [e.g., *Blanke et al*., 2001; *Speich et al*., 2001, *Koch-Larrouy et al*., 2008; *Lique et al*., 2010]. The method is presented in detail and discussed by *Blanke & Raynaud* [1997] and *Blanke et al*. [1999].

[12] In our experiment, we deploy Lagrangian particles at the depth of 65 m on a regular grid across the AO. We perform a backward tracking (i.e., reverse time) of the particles until they reach three geographical interception sections that define the three main inflow routes into the AO: Bering Strait, Fram Strait, and Barents Sea opening at 20ºE. The 65 m depth horizon was chosen as an estimate of the maximum depth of upper ocean mixing throughout the year. Thus, we effectively assume that nutrient concentrations at approximately this level determine the vertical entrainment of nutrients and thus define the availability of nutrients for phytoplankton to utilize at the beginning of the light season. All the particles were released simultaneously on 1 January. A number of short sensitivity experiments with release at different times of the year showed low sensitivity of the averaged advective timescales to the date of the release.

2.3. Productivity Data Base

[13] We quantified the contribution of the SCM using in situ Chl-a data from the Arctic System Science Primary Production (ARCSS-PP) database [http://accession.nodc.noaa.gov/0063065; *Arrigo et al*., 2011]. All profiles north of 66ºN were interpolated onto a regular vertical grid. We assumed an average UML depth of 20 m and estimated the contribution of the subsurface Chl-a maximum as a fraction of the biomass below UML to the total biomass in the water column. Note that although the data base contains large number of observations, they do not provide a good coverage neither for the deep AO nor for a typical AO annual cycle (Figure 2). The data coverage is especially poor for the central Arctic, East Siberian Sea, and Canadian Arctic Archipelago (CAA) and observations are absent for the Laptev Sea.

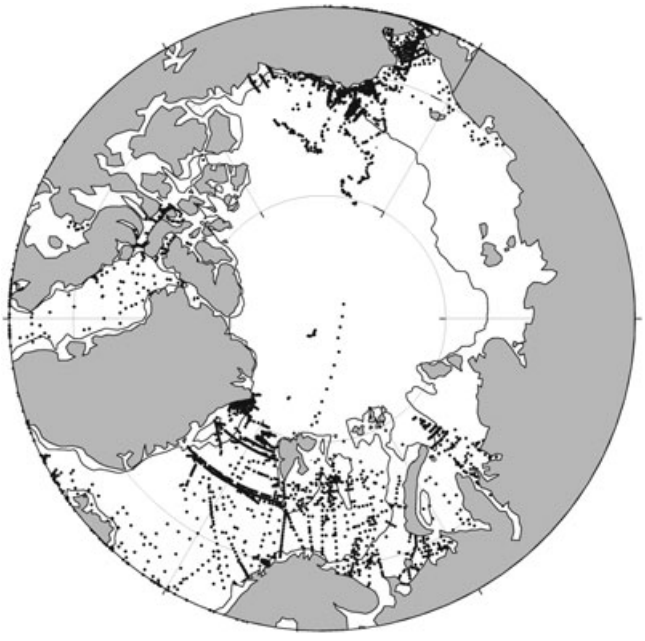

Figure 2. Location of the Chl-a vertical profile observations included into ARCSS data base.

3. Results

3.1. Simulated Sea Ice, Ocean Circulation, and Water Masses

[14] A detailed model assessment in respect to the AO circulation, sea ice, distribution of key water masses, and oceanic exchanges with the North Atlantic and North Pacific has been done within the framework of the AOMIP [*Proshutinsky et al*., 2011, *Popova et al*., 2010, 2012]. Here we present a brief description of the simulation results that are relevant to the present study.

[15] Simulated annual sea-ice extent for 1979–2007, integrated over the whole AO ($12.7\pm2.8\ 10^6$ km^2) is within 3% of the passive microwave satellite data from the National Snow and Ice Data Center [Boulder, CO, USA; *Cavalieri et al*., 1996]. The simulated long-term downward trend in sea-ice extent is lower than that observed ($-238{,}990$ km^2 decade^{-1} vs. $-443{,}120$ km^2 decade^{-1}). Excess sea ice in NEMO occurs during winter months, and summer sea-ice trends in NEMO are similar ($-428{,}090$ km^2 decade^{-1} and $-376{,}890$ km^2 decade^{-1}) to those in Pan-Arctic Ice Ocean Modeling and Assimilation System [e.g., *Zhang and Rothrock*, 2003; *Schweiger et al*., 2011]. The spatial distribution of simulated September sea-ice concentrations is similar to the sea-ice concentration retrievals from passive microwave satellite data using NASA Team algorithm [*Cavalieri et al*., 1996], although the HadISST dataset [*Rayner et al*., 2003] shows more summer sea ice than both NEMO and the passive microwave data [cf. Figures 2 and 3 in *Popova et al*., 2012]. For the 1979–2006 period, total sea-ice volume simulated by NEMO is $24.3\pm6.2\ 10^3$ km^3 which is approximately 12% higher than that estimated by PIOMAS ($21.7\pm6.2\ 10^3$ km^3). However, the correspondence with observations significantly improves if only the later period 1995–2007 is considered. Therefore, NEMO is likely to have a statistically significant positive bias in Arctic sea-ice volume prior to the 1990s, but that this diminishes post-1990. Since the LIM2 model does not have an explicit

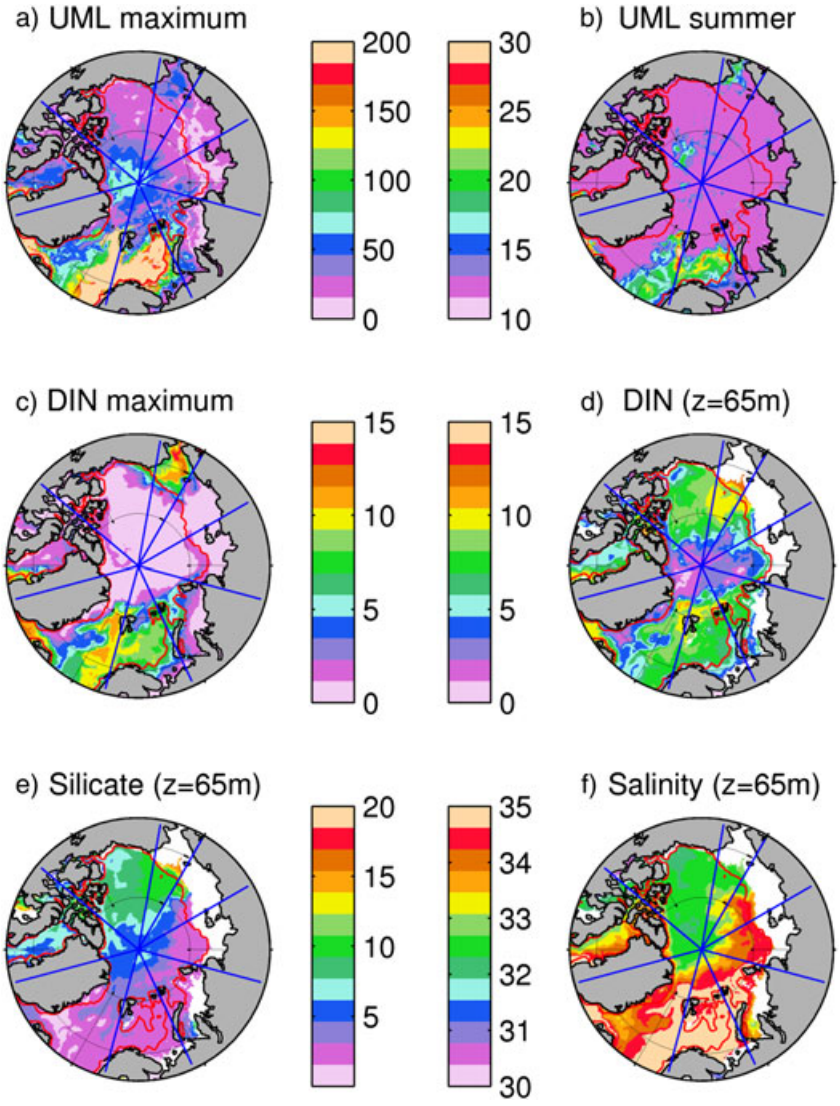

Figure 3. Model results for year 2006: a) Summer (June-August) averaged UMl depth, b) maximum depth of UML during the year on the basis of monthly averaged values; c) maximum DIN concentrations (mmol N m^{-3}) on the basis of monthly averaged values; d) DIN concentration at depth of 65 m.

formulation of the meltponds evolution but a parameterization of the light penetration through the ice in the water column [*Fichefet and Morales Maqueda*, 1997], it underestimates light penetration in the ice pack areas in summer when snow is melted. However, the bias is small since the presence of thin layer of snow effectively cuts off the light penetration in the sea bulk [e.g., *Taylor and Feltham*, 2004].

[16] Tables 1 and 2 show comparisons of simulated and observed oceanic exchanges between the AO, the North Atlantic and the North Pacific. Overall, NEMO demonstrates good skill in simulating Arctic exchanges—model transports are within the range of observational uncertainties. The only bias is an excessive simulated inflow through the Bering Strait, resulting in increased buoyancy of water masses in the Chukchi Sea (Table 2).

[17] Following the approach taken by *Clement Kinney et al*. in press, 2012, we have compared the near-bottom temperature and salinity of the inflow through Bering Strait at the long-term moorings A2 and A3 with the corresponding virtual model stations and find that modeled properties are in good agreement with observations. The simulated properties of Atlantic water inflow into the Barents Sea also agree well with measurements (Table 2). The spatial structure of the Barents Sea outflow in NEMO is similar to that simulated by other high-resolution models [e.g., *Aksenov et al*., 2010a, 2011]. In NEMO, most of the outflow of water from the Barents Sea into the Eurasian basin of the AO occurs through the eastern St. Anna Trough as a bottom-intensified boundary current. In this region, the simulation is consistent with recently obtained mooring data and Conductivity-Temperature-Depth measurements; these have been discussed in detail elsewhere [*Kirillov et al*., 2012].

[18] The simulated ocean circulation in the top 100 m (which includes both the UML and the upper halocline) is cyclonic (counter-clockwise) in the Eurasian Basin (Nansen and Amundsen Basins) and in the Makarov Basin of the AO (here we refer to the mean model state, averaged for 1979–2006). The Transpolar Drift is along the Mendeleev-Alpha Ridge, with an anticyclonic (clockwise) Beaufort Gyre in the Canada Basin being reduced. This circulation creates a "cyclonic" type regime in the AO and is associated with reduced atmospheric pressure over the Beaufort Sea. The period 1979–1988 corresponds to the negative Arctic Oscillation indices, whereas the period 1989–2006 corresponds to positive and neutral Arctic Oscillation indices [e.g., *Steele et al*., 2004; *Proshutinsky and Johnson*, 1997]. During the former period, model circulation features a stronger Beaufort Gyre and Transpolar Drift aligned with the Lomonosov Ridge. During the latter period, the Beaufort Gyre is weaker and Atlantic Water inflow spreads further east into the AO [*McLaughlin et al*., 1996]. At the depth range of this Atlantic Water, 100–500 m, the main circulation feature in the model is the Arctic Circumpolar Boundary Current which follows the AO margins cyclonically. This is the fastest oceanic jet in the model AO, with annual mean velocities up to 0.1 m s^{-1}, consistent with other high-resolution models and with observations [*Aksenov et al*., 2011]. The boundary flow in NEMO is stable in the Eurasian and Makarov Basins but slows down considerably downstream towards Canada Basin, exhibiting variability in strength and flow direction similar to both other simulations and observations [*Karcher et al*., 2012].

[19] Summarizing this section, we conclude that the model has necessary skill to accurately simulate ocean and sea-ice features of the AO.

3.2. AO UML Dynamics and Nutrients

[20] Modeled annual maximum UML depth (calculated from monthly averaged values) is shown in Figure 3a. Deep winter mixing (in excess of 300 m) in the model occurs only in the Atlantic inflow waters in the southeast Greenland and southwest Barents sectors. Winter mixing rarely exceeds 80 m outside of these areas and on average is only 40 m being generally deeper in the Eurasian than in Canadian basins [e.g., *Alkire et al*., 2007; *Rudels et al*., 2004; *Timmermans et al*., 2011]. Modeled summer (averaged over the period May-September) UML depth is shown in Figure 3b. With the exception of the Atlantic inflow (Norwegian and southern Barents Seas), its depth does not exceed 10–15 m in the central AO. In the weakly stratified Norwegian and Barents seas,

Table 2. Mean 1979–2007 Simulated in NEMO 1/4° Characteristics of the Atlantic Water (AW) Inflow in the Arctic Ocean Through Fram Strait and the Barents Sea Opening and These of the Pacific Water (PW) Flow Through Bering Strait[a]

Strait:	AW in Barents	PW in Bering[b]
Volume [Sv]	2.1 ± 0.5 **(2.0 ± 0.4)**	1.3 ± 0.2 **(0.8 ± 0.2)**
Heat [TW]	42 ± 12 **(50 ± 10)**	16 ± 0.2 **(12 ± 0.3)**
FW [mSv]	-10 ± 4 **(-5.7)**	94 ± 11 **(80 ± 10)**
Mean T [°C]	3.2 ± 0.5 **(2.8–3.9)**	0.26 **(0.27)** 0.09 **(-0.11)**
Mean S	34.95 ± 0.05 **(34.84)**	32.30 **(32.26)** 32.47 **(32.49)**

[a]The corresponding observational estimates from a variety of bibliographic sources are given in bold [*Rudels et al*., 2004; *Fieg*, *et al*., 2010; *Gammelsrod et al*., 2009; *Smedsrud et al*., 2010; *Tsubouchi et al*., 2012; *Clement Kinney et al*., in press, 2012]. Where possible standard deviations of the transports are given. Note that observational uncertainties are included in the standard deviations. Positive transports are into the Arctic Ocean. The heat (temperature) transports are referenced to −0.1°C; freshwater transport is referenced to 34.8.

[b]In Bering Strait, temperature and salinity were recorded at the moorings A2 and A3 at 10 m above seabed; the corresponding model virtual stations were sued for comparison [for details, see Clement *Kinney et al*., 2012].

Table 1. Mean 1979-2007 Simulated in NEMO 1/4° Oceanic Transports Through the Key Arctic Straits and Observational Estimates (in Bold) From a Variety of Bibliographic Sources[a]

Strait:	Fram	Barents	Davis Strait
Volume [Sv]	-1.2 ± 0.6 **(-1.8 ± 5.0)**	2.4 ± 0.5 **(2.8 ± 0.6)**	-2.8 ± 0.6 **(-2.6 ± 1.0)**
Heat [TW]	40 ± 11 **(36 ± 6)**	72 ± 11 **(73)**	27 **(20 ± 9)**
FW [mSv]	-41 ± 8 **(66 ± 18)**	-10 ± 4 **(-9 ± 2)**	-122 ± 17 **(-116 ± 41)**

[a]Aksenov *et al*. [2010b], Fieg, *et al*. [2010], Beszczynska-Moeller *et al*. [2011], Curry *et al*. [2011], and Tsubouch *et al*. [2012]. Where possible, standard deviations of the transports are given. Note that observational uncertainties are included in the standard deviations. Positive transports are into the Arctic Ocean. The heat (temperature) transports are referenced to −0.1°C; freshwater transport is referenced to 34.8.

summer UML is substantially deeper (20–30 m). Both summer-averaged and winter maximum UML values show features similar to ones obtained from the WOA climatology using variable density criterion [*Popova et al*., 2010].

[21] The modeled annual maximum of surface dissolved inorganic nitrogen (DIN) concentration is shown in Figure 3c. This characteristic is of importance as it is indicative of the amount of nutrients available for phytoplankton to utilize in the UML at the beginning of the spring bloom. The majority of the central AO and Siberian shelves show low concentrations of 1–2 mmol N m^{-3}. Areas close to the Pacific and Atlantic inflows are clear exception from this rule. Chukchi and Norwegian Seas show high DIN concentrations of about 8–12 mmol N m^{-3} while DIN in the Barents Sea is about 6–10 mmol N m^{-3}. Although the AO is severely undersampled in respect to nutrients [e.g., *Popova et al*., 2012], the annual maximum of DIN obtained from the World Ocean Atlas' monthly nutrient climatology [*Garcia et al*., 2006] shows similar patterns of spatial distribution [*Popova et al*., 2010; 2012].

[22] The modeled annual DIN concentrations at 65 m depth are shown in Figure 3d. The distribution and origin of DIN at this depth are the main focus of our analysis. Similar to surface maximum DIN concentrations, elevated values can be found in the vicinity of the Pacific and Atlantic inflows. However, unlike the surface distribution, at this depth, DIN concentrations in the Eurasian Basin are substantially lower (1–5 mmol N m^{-3}) than in the Canada Basin (6–11 mmol N m^{-3}). Extremely low values (<1 mmol N m^{-3}) occur in the northern part of the Greenland sector.

[23] Silicic acid concentrations at this depth (Figure 3e) show spatial features that are very different from DIN and reflect the fact that Pacific inflow is has much higher silicic acid concentrations (20–25 mmol Si m^{-3}) than the Atlantic inflow [6–10 mmol Si m^{-3}, *Garcia et al*., 2006]. Modeled silicic acid concentrations at the depth of 65 m vary between 9–10 mmol Si m^{-3} in the Canada Basin and 2–5 mmol Si m^{-3} in the Euroasian Basin. This distribution follows inverse distribution of salinity at the same depth (cf. Figures 3e and 3f) which at this depth is a good tracer for waters of Pacific origin [e.g., *Jones et al*., 2003]. Thus, modeled silicic acid concentration is much higher in the Pacific waters with general decline (due to biological consumption) downstream of the Bering Strait reaching a minimum (~5 mmol Si m^{-3}) in the northern part of the reenland sector. Because, by contrast, Pacific and Atlantic inflows have similar DIN concentrations [6–10 mmol Si m^{-3} at 50 m depth; *Garcia et al*., 2006], understanding of the DIN distribution shown in Figure 3d (in particular, the striking difference between the Canadian and Eurasian basins) requires analysis of the advective pathways and timescales involved. This analysis is described in the next section.

[24] The modeled and observed [WOA05, *Garcia et al*., 2006] cross sections of DIN are shown in Figures 4a and 4b. As can be seen, the model reproduces well the strength and depth of the nutricline, although it tends to underestimate surface concentrations and is more oligotrophic than the climatology. However, the number of actual observations used in the climatology from the central Arctic is insufficient [cf. Figure 6 in *Popova et al*., 2012] to confirm if the differences between the Canadian and Eurasian basins are reproduced correctly by the model. Further model evaluation with respect to observed nutrients can be found in *Popova et al*. [2010].

3.3. Lagrangian Analysis of Nutrient Supply to the Upper Halocline

[25] In order to estimate the advective timescales affecting supply of nutrients to AO ecosystems and the geographical

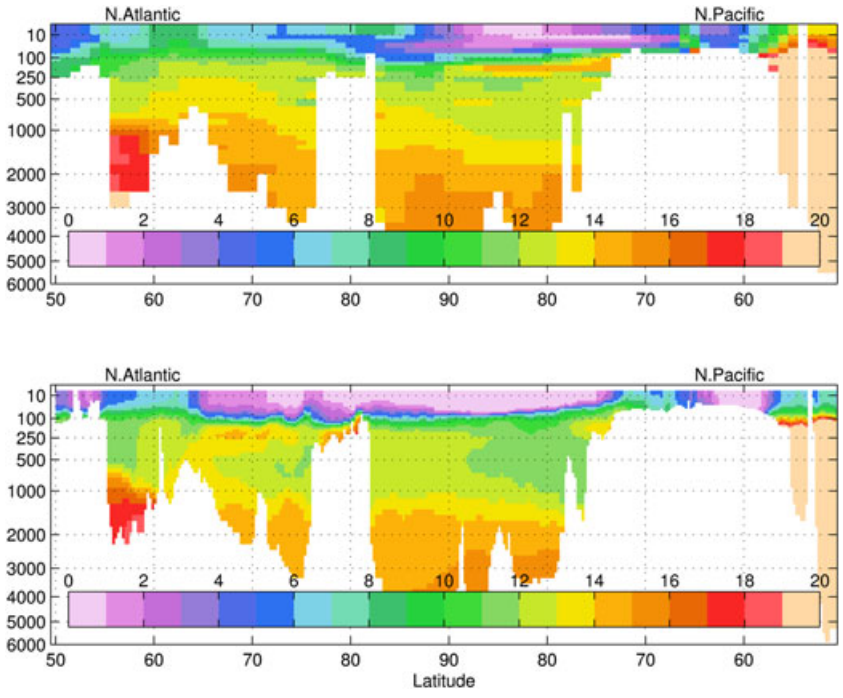

Figure 4. Vertical cross section of annual mean DIN concentration a) WOA; b) model results (year 2000, mmol N m^{-3}). Location of the cross section is shown in Figure 1.

sources of nutrients, we deployed Lagrangian particles at a depth of 65 m across the AO and performed backward tracking (see section 2.2) until they reached one of three interception sections shown on Figure 1: Bering Strait, Fram Strait at 80ºN and the opening of the Barents Sea at 20ºE. The 65 m depth horizon (bounded by the model vertical grid at 56 and 69 m) was chosen as a depth generally below the maximum depth of upper ocean mixing through the year (cf. Figure 3a), while still being within the photic zone. Hereafter, we will refer to this experiment as Z65. Note that our experiment is designed to establish the main routes of nutrient circulation in the AO and the timescales involved. Our approach is not designed to provide flux estimates for water and nutrients.

[26] Figures 4a–c show the origins of the particles arriving to the depth of 65 m and a timescale required for particles to be advected from one of the three entry sections. We discuss the results separately for each of the entry sections. Note that henceforth, we refer to ARIANE particles as "water parcels".

3.3.1. Pacific Water

[27] Figures 6a and 6d show Lagrangian trajectories of particles of the Z65 experiment colored according to their depth and DIN concentration. After entering via the shallow (50 m) Bering Strait, and crossing the shelves of the Chukchi Sea and East Siberian Sea in the top 50 m of the water column, Z65 water parcels are subducted under the lighter AO surface water to depths of 50–100 m at the shelf break. Lower part of the 50–100 m depth range is occupied by the water parcels that become denser as a result of brine rejection during ice formation.

[28] Observations suggest that shelf-slope convective plumes can penetrate deeper [e.g., *Jones et al.*, 2003; *Anderson et al.*, 2010]; however, our analysis finds that only water parcels subducted to depths shallower than 100 m will eventually end up at the reference depth of 65 m, while water parcels subducted deeper will stay below the photic zone throughout their advection across the AO. At the depth of 65 m (Figure 5a) Pacific water fills the Chukchi and Beaufort Seas, Canada Basin, and sills of the CAA.

[29] Water parcels entering the AO through the Bering Strait have high nutrient concentrations ranging from 5–7 mmol N m^{-3} in summer to 12–15 mmol N m^{-3} in winter, with the exception of more nutrient-depleted Alaskan coastal current water parcels that have concentrations of 4–6 mmol N m^{-3} (Figure 6d). Advection from the Bering Strait to the Chukchi shelf break takes on the order of 1–2 years (Figure 5a). As water parcels cross the Chukchi Sea shelf, DIN decreases such that at the shelf break it is only 9–12 mmol N m^{-3}. This decrease is relatively low for an area of high primary production (~150–200 g C m^{-2} yr^{-1}). This is explained by the fact that the surface nutrient concentrations (Figure 3a) are high in the southern part of the Chukchi sector, and majority of the production occurs within the UML while the SCM is relatively weak because of the self-shading effect. Relative strength [*Popova et al.*, 2010] of the SCM increases from the shelf break northward [*Hill & Cota*, 2005; *Popova et al.*, 2010] where a further decrease in nutrient concentrations occurs.

[30] Analysis of the individual water parcels shows that three main routes can be clearly established: transpolar drift, surface anticyclonic circulation of the Beaufort Gyre, and a branch that follows the coast of North America. Transpolar drift of Z65 water parcels from the Bering Strait to the Greenland shelf takes 6–10 years (Figure 5) and generally

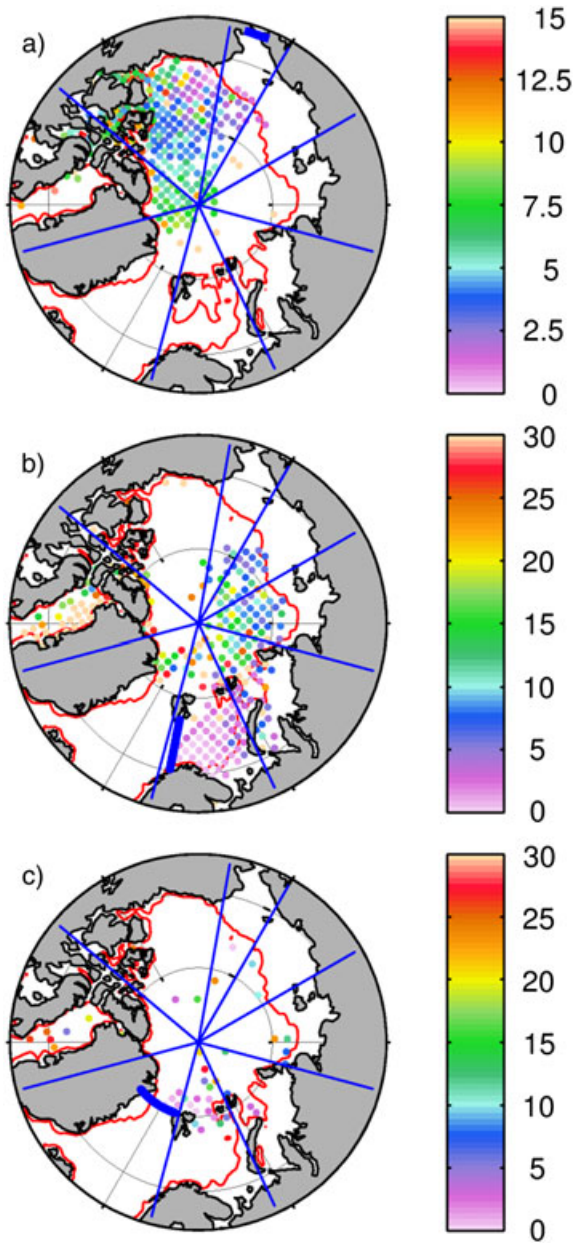

Figure 5. Origin of the Lagrangian trajectories at 65 m depth and time (in years) required to reach the shown location from one of the three entry points: a) Bering Strait; c) Barents Sea opening; d) Fram Strait.

occurs at depth of 60–80 m. After leaving the shelf break of the Chukchi Sea, water parcels caught in the Transpolar Drift experience progressive reduction in their DIN concentrations (about 1–2 mmol N m^{-3} yr^{-1}), such that in the area north of Greenland, their DIN concentration is only 1–2 mmol N m^{-3}. Thus, the minimum of DIN north of Greenland (Figure 3d) is explained by the downstream depletion of the Pacific nutrient source.

[31] Water parcels following the northern coast of Alaska enter the AO with relatively low nutrient concentrations of 4–6 mmol N m^{-3}. They remain in near-surface layers (0–40 m) until reaching transverse of McKenzie river whereupon they downwell to depths of 60–80 m and recharge their nutrients to 6–10 mmol N m^{-3} through the

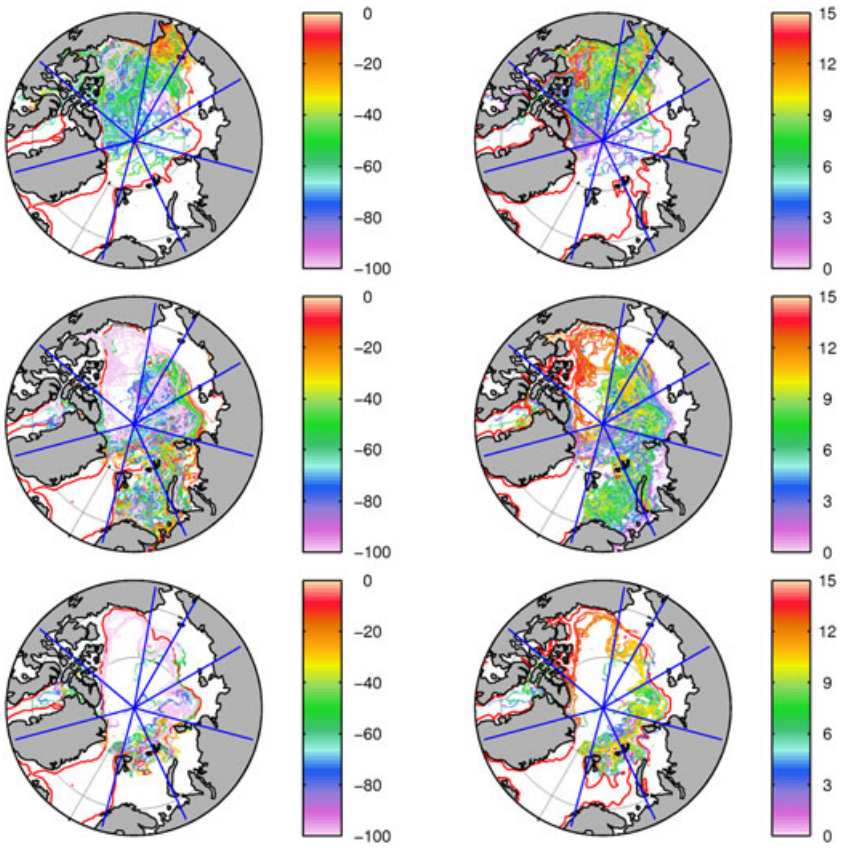

Figure 6. Lagrangian particles colored according to their depth (m) and DIN concentration (mmol N m^{-3}) shown separately for each of the entry routes: (a and d) Bering Strait, (b and e) Barents Sea opening, (c and f) Fram Strait.

remineralization of the particular organic matter before penetrating the sills of the CAA and reaching Baffin Bay. Advection from the Bering Strait to the sills of the CAA occurs on a timescale of 10–12 years, and to Baffin Bay on a timescale of 15–20 years depending on the route taken through the CAA. Longer timescales of Arctic residence (20–25 years) are indicated by some water parcels (5%) which were caught in the Beaufort Gyre motion. Above timescales are similar to published transit times required for surface and subsurface waters to across the AO [e.g., *Newton et al.*, 2008]. General features of the circulation discussed here (and in the next two subsections) are shown on the schematic diagram of Figure 7.

3.3.2. Atlantic Water

[32] Water parcels entering through the opening of the Barents Sea traverse it in the model on a timescale of 3–5 years experiencing atmospheric cooling and salinification when sea ice is formed. These processes are believed make seawater dense enough to flow off the shelf in plumes that spread through a wide range of depths [*Jones et al.*, 1998; *Rudels et al.*, 2004]. Because of its high productivity, the Barents Sea acts as a sink of nutrients in the upper 0–120 m, such that water parcels entering it with a typical DIN concentration of 8–10 mmol N m^{-3} (at the depth of 65 m) leave it with only 6–7 mmol N m^{-3} if they remain at the same depth (Figure 3d). In our analysis, Z65 water parcels exit the Barents Sea mostly through the passage between Franz Josef Land and Novaya Zemlya or via the narrow and shallow Kara Gate. Both the

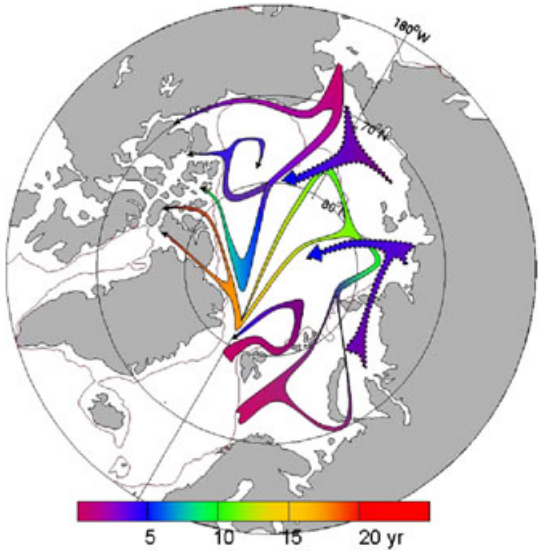

Figure 7. Schematic diagram of the advective pathways of the nutrient supply to the subsurface waters of the AO. Arrows are colored according to the time (in years) required to reach the shown location from one of the three entry points.

pathways eventually lead in the Arctic and Ocean via the St. Anna Trough in the Northern Kara Sea with a small fraction of parcels entering the Laptev Sea through the Vilkitsky Strait (Figures 6b and 6e). This pattern of the flow is similar

to the one observed in the St. Anna Trough [*Kirillov et al*., 2012]. In the AO, the water parcels follow the continental shelf and join the cyclonic circulation of the Makarov and Amundsen Basins at a depth of 60–100 m spreading through both the basins on timescales of 10–20 years (Figures 5b and 7). In general, water parcels in the Makarov Basin show higher nutrient concentrations (4–6 mmol N m^{-3}) than in Amundsen Basin (0.1–3 mmol N m^{-3}) while occupying approximately the same range of depths.

[33] Another deeper branch (180–200 m) continues along the continental shelf and into the Canada basin under the Pacific water and upwells on the shelf of Greenland due to the gradual thinning of the Pacific water layers [*Rudels et al*., 2004]. This shallowing allows some of the Barents branch water to enter Baffin Bay through the sill in the Nares Strait (230 m). The timescales involved in the transition from leaving the Barents Sea and arriving at the Canadian and Greenland shelves are about 20–30 years.

[34] In the circulation pattern described above there are a number of areas where water parcels increase their nutrient concentrations within the AO. One of the two mechanisms of such increase is associated with the fact that remineralization of the organic matter occurs throughout the water column (source of DIN), while consumption of DIN is bound to the photic zone only. Thus, particles being advected in the lower part of the water column generally increase their DIN concentration, while they lose DIN in the photic zone. The exact depth at which biogeochemical sources of DIN change its sign is largely driven by the light regime (hence latitude and the season) and nutrient concentrations both of which control productivity level. The second mechanism is associated with the turbulent mixing which is disregarded by the off-line Lagrangian calculations but is present in the full model. For instance, if the Lagrangian particle crosses the area affected by the deep convection, associated DIN will show increase of the concentration. In the Atlantic inflow, the first of such areas is in an area east of Novaya Zemlya where deep winter convection is observed [e.g., *Aksenov et al*., 2010b; *Arthun et al*., 2011 and occurs in the model. In this area, DIN concentrations increase from 2–3 to 6–8 mmol N m^{-3}. However, this increase is mostly utilized in the surface waters of the outer Kara shelf. The next downstream enrichment of nutrients occurs after water parcels leave the shelves of Barents and Kara Seas and increase their DIN concentrations from 5–6 to 7–10 mmol N m^{-3}, presumably due to mixing with high nutrient bottom shelf waters (discussed in detail in the next section). The last substantial enrichment of nutrients occurs on the border between the Chukchi and East Siberian sectors where the shelf circumpolar current separates from the Siberian shelf and descends below Pacific-origin waters. In this area, Z65 water parcels downwell to depths of 60–80 m and restore their DIN concentrations to 6–9 mmol N m^{-3} due to the remineralization of the organic matter.

[35] Water parcels entering the AO through the Fram Strait feed the upper halocline of the western Nansen Basin (Figures 5c, 6c, and 6f). The majority of the water parcels stay within the upper 60–80 m and transverse the Nansen Basin on a timescale between 3 and 8 years. On their route across the Nansen Basin, water parcels lose on average approximately 1 mmol N m^{-3} yr^{-1}. However, a number of water parcels experience strong downwelling north of Svalbard, at which point they join cyclonic circulation of the intermediate waters in AO and can be upwelled to our reference depth along the shelf of Greenland and the CAA and can, in some cases, reach Baffin Bay. In the case of the Baffin Bay, the timescales involved are between 20 and 30 years dependent on the particular route taken.

[36] High DIN concentrations (9–12 mmol N m^{-3}; Figure 6) supplied to the western Nansen Basin through the Fram Strait result from deep convective mixing in the Norwegian and Greenland seas (cf. Figures 3a and 3b). In this area, high DIN concentrations are supplied to the surface every year during the winter mixing and are subsequently advected by the cyclonic circulation to the majority of the Nansen Basin on the timescales of 2–5 years (Figure 7). Taking into account this deep source and the short advective timescale of DIN supply to the majority of the Nansen Basin, we can speculate that further sea-ice retreat in this area may lead to substantial increases in productivity. In this respect, Nansen Basin presents a rather unusual example for the AO. Over the rest of the basin dominated by predominantly horizontal supply, ice retreat leading to in situ increase of productivity follows by draw down of nutrients and subsequent decrease of production in the downstream areas.

[37] Our estimates of advective timescales for the Atlantic Water in the Eurasian Basin of the AO are consistent with the estimates of *Smith et al*. [2011] based on their time-series measurements of the nuclear fuel reprocessing tracers Iodine-129 and Cesium 137 and CFC-11 data. These authors have obtained travel time between the Barents Sea and North Pole of ~8 years for the tracers and estimated the age of AW in the Makarov Basin of 12–20 years and in the outflow through Fram Strait of 30–40 years. As part of the Arctic Monitoring and Assessment Program, *Karcher et al*. [2012] obtained residence times of the Arctic halocline of ~10 years, for the AW of ~25–30 years. Independently, *Ekwurzel et al*. [2001] estimated the age of halocline waters (top 250 m) of ~ 10 years using 3H-3He tracers.

3.3.3. Continental Shelf Pump

[38] The Lagrangian experiments described in the previous sections were not designed to consider another possible source of nutrients for the AO halocline, namely nutrients supplied to shelf bottom waters by the remineralization of sinking organic particles [e.g., *Jones & Anderson*, 1986). To elucidate the role of this mechanism in sustaining AO primary production, we performed an additional simulation in which the return of remineralized particulate organic matter to inorganic nutrients in the bottom model grid box was (globally) disabled (i.e., particular organic matter was remineralized, but the nutrients "disappeared"). A simple interpretation of this experiment is that the ocean bottom starts acting as a trap for the sinking organic material and bottom of the shelves are no longer areas of high nutrient concentrations. In a sufficiently long simulation, the results of this experiment would be confounded by the depletion of inorganic nutrients, but on the timescale of a decade, this experiment has two impacts that help elucidate the role of shelf bottom waters in nutrient resupply. Namely: (i) an in situ impact on the productivity of shallow shelves, and (ii) a remote impact on areas controlled by the shelves through advection of bottom shelf waters. One might expect the effect to be restricted to the remote advective mechanism only (outside of areas where bottom topography is within

the photic zone), since strong stratification in the AO shelf areas means that they are typically not mixed down to the seafloor (i.e., do not tap into shelf bottom nutrients). As such, this extra simulation is used here to provide information on the role of shelf bottom waters in supplying the AO thermocline. Note that, due to the computational expense of the model, this experiment is performed at 1º resolution (see Methods).

[39] AO primary production from the control run and its relative reduction in the numerical experiment after 6 years are shown in Figure 8. As can be seen in Figure 8b, the impact on productivity propagates far beyond the shelf into the central AO. In particular, there are two pronounced large-scale filaments of decreased productivity: northwestern flow from the Laptev shelf into the Amundsen basin, and northeastern flow from the East Siberia shelf into the southern part of the Makarov Basin and the Canada Basin. In these basins, primary production is reduced by a factor of two over significant areas (Figure 8b). Further analysis shows that the total impact of this mechanism on AO primary production saturates after 5–6 years at approximately a 20% total (cumulative) reduction.

[40] To explain the spatial pattern of reduced primary production, we performed a Lagrangian experiment tracing the propagation of the shelf bottom water. We placed Langrangian particles into the bottom grid cells over the shelf area (<220 m) in all model grid points north of 66ºN and traced their advection forward in time for 5 years. The resulting water parcel trajectories, colored according to their depth, are shown in Figure 9a. To simplify interpretation of the advective routes, the same water parcels colored by their starting sector are shown on the Figure 9b [geographical sector boundaries are taken from *Pabi et al*., 2008]. Water parcels starting from the outflow shelves of the Baffin and Greenland sectors (shelf classification per *Carmack et al*., 2006] are omitted from the figure for simplicity as they are not relevant to the discussion. Only water parcels whose trajectories bring them to a depth shallower than 100 m are shown in the subplots of Figure 9 as deeper trajectories would have very limited or no impact on AO productivity.

[41] The results show that all of the shelf waters join the cyclonic circulation of the Arctic shelf boundary current [*Aksenov et al*., 2011] that flows around the rim of the AO, entraining waters cascading from the Arctic shelves and making detours around topographic features [*Aksenov et al*., 2011]. In particular, the water parcel trajectories show that shelf water from the Barents sea and the outer shelf of the Kara sea join the ASBB at a depth below 200 m, and they remain below this depth either for the duration of the run (5 years) or until they reach shelves of CAA and thus

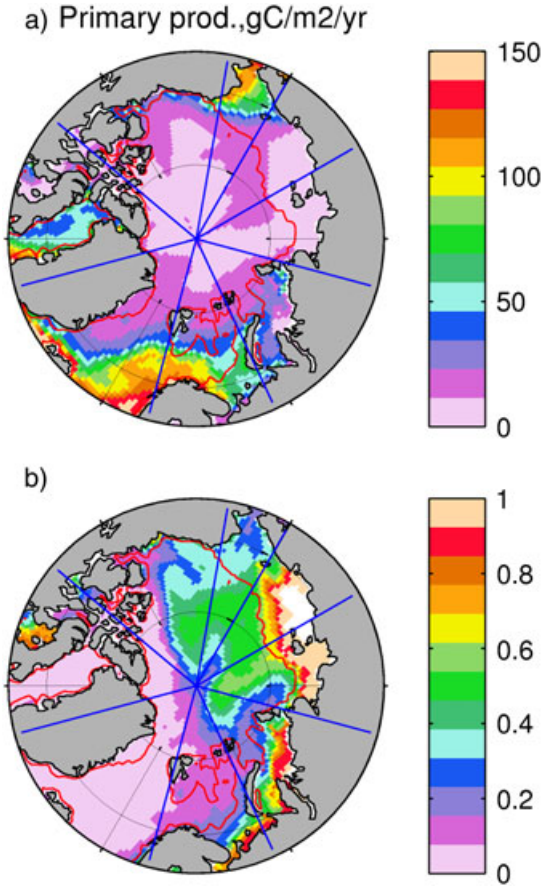

Figure 8. (a) Annual mean water column primary production in the control run (mg C m^{-2} yr^{-1}); and its relative reduction after six year of the shelf control experiment (b) calculated as (control-experiment)/control.

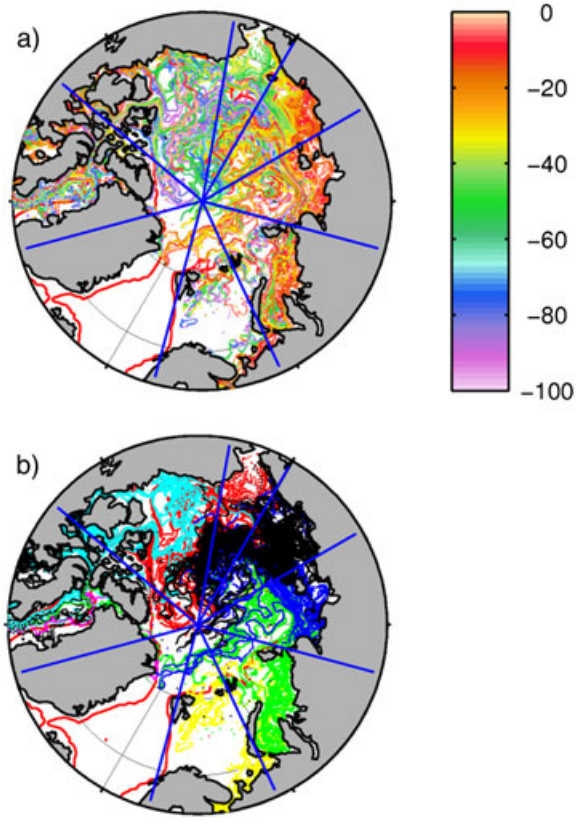

Figure 9. Lagrangian trajectories starting in the model shelf points and run forward for 6 years colored by (a) depth and (b) sector of origin (yellow: Barents, green: Kara, Blue: Laptev; black: East Siberian; red: Chukchi; cyan: Beaufort). Only parts of the trajectories remaining above 100 m depth are shown.

do not influence productivity of the AO. Inner shelf waters of the Kara Sea exit it only through the Kara Gate into the Laptev Sea thus explaining why Barents and Kara shelves do not control primary production in the deep AO of their corresponding sectors.

[42] The main advective path found in the model for the off-shelf nutrient-enriched flow formed in the inner shelf of the Kara Sea and on the shelf of the Laptev Sea is a cyclonic circulation of the Amundsen Basin (Figure 9) at a depth of 40–60 m. This pattern of shelf-basin exchange explains why the Amundsen Basin has higher DIN concentrations in the Z65 experiment than does the Nansen Basin. In the Amundsen Basin, the timescale of advective nutrient supply from the Barents Sea opening is 10–15 years, while shelf supply mechanism operates on the timescale of 3–5 years.

[43] Finally, the East Siberian and Chukchi sea shelf waters join the ASBB and penetrate into the deep AO through its separation from the shelf near the Chukchi Plateau. This branch of shelf flow stays at depth 80–100 m (just below Z65 waters).

[44] The timescale of shelf-basin exchange of near-surface waters in our model (~5 years) is similar to the observational estimates by *Schlosser et al*. [1999], *Serreze et al*. [2006] and *Rutgers van der Loeff et al*. [2012].

4. Discussion

[45] The supply of nutrients to the upper ocean ecosystems has traditionally been attributed mostly to vertical processes such as vertical diffusivity, winter convection, upwelling, and mesoscale eddy pumping. As was pointed by *Palter et al*. [2005], such a one-dimensional view rests on the assumption that an adequate reservoir of nutrients is perennially available under the photic zone and neglects lateral processes that deliver nutrients to the subsurface. In general, a number of studies [e.g., *Sarmiento et al*., 2004; *Palter et al*., 2005] have found that, on timescales longer than a decade, the horizontal processes that control the vertical distribution of nutrients must be taken into account. However, horizontal processes become important on much shorter timescales in the AO because of its restricted vertical exchange processes, wide continental shelves, and strong horizontal gradients of nutrients with the neighboring northern North Pacific and Atlantic basins.

[46] In order to estimate the timescales associated with horizontal transports of nutrients to AO ecosystems, here we marry conventional Eulerian simulation output with Lagrangian tracer experiments. Although Lagrangian particle tracking has its limitations for studying tracer distributions since it disregards mixing process, its use in the AO is arguably more justifiable than in other ocean areas. Using time-series measurements of nuclear fuel reprocessing tracers and a ventilation tracer (CFC-11), *Smith et al*. [2011] showed that advection may play a greater role than mixing in distribution of tracers in the AO, and that AO is a more advectively dominated system than neighboring North Atlantic and Pacific oceans.

[47] We focused our analysis at the origin of the water at depth of about 65 m (Z65 water). We assumed that supply of nutrients to this depth is of major consequence for the AO ecosystems for two reasons. First, the concentration at approximately this level determines vertical entrainment of nutrients into the UML and thus defines how much nutrient is available for phytoplankton to utilize at the beginning of the light season in the UML, although care should be taken in areas most strongly affected by the fresh water input where winter mixing may not penetrate to this depth. Second, nutrients at this depth support a subsurface Chl-a maximum which is a prominent feature of the AO ecosystems and responsible for a significant proportion of total AO primary production *Popova et al*. [2010]; *Martin et al*., 2010]. Our results showed that DIN-enriched Pacific waters entering the AO through the Bering Strait fill the Canada Basin and the western Amundsen Basin on the timescale of 5–10 years. In areas where the transient time is the longest (~10 years, western Amundsen Basin), the waters are "biologically spent" and have DIN concentrations close or below the phytoplankton half-saturation level for nutrient uptake. These results also show connectivity between surface processes in the Chukchi Sea and downstream subsurface areas of the Canada Basin. For example, they suggest that the earlier sea-ice retreat affecting progressively larger areas on the Chukchi shelf observed over the last decade leads to increased surface productivity [*Arrigo et al*., 2008] followed by reduction of surface nutrients that may have a strong downstream impact on the SCM of the CB on the timescale of 3 to 5 years. Surface waters over the Chukchi shelf are feeding the subsurface productivity of the nutrient-poor CB and along the transpolar drift. Our results also suggest that the downstream effect may not propagate as far as CAA and Beaufort Sea as a "recharge" of the nutrients occurs on the shelf of Greenland and CAA due to the shelf-break upwelling. Recently, *McLaughlin & Carmack* [2010] showed deepening of the nutricline and SCM because of the accumulation of the fresh water in the surface BG in 2003–2009 due to increased sea-ice melt and wind-driven convergence. On the basis of our results, we can speculate that this deepening may be further exacerbated by the enhanced nutrient consumption upstream in the Chukchi Sea.

[48] Similar to the "biologically spent" waters of the western Amundsen supplied from the Bering Strait, subsurface waters of the eastern Nansen Basin are also depleted of nutrients. This depletion is due to the long advective timescales between the North Atlantic (through the Barents Strait) and Nansen Basin. In contrast to the eastern Nansen Basin, the eastern Makarov and Amudsen basins have higher subsurface DIN concentrations in spite of the similar advective scales from the Atlantic sources. In this case, nutrients are enriched by the continental shelf pump which supplies shelf bottom waters with high nutrient concentrations to the subsurface layers on the timescale shorter than that from the North Atlantic.

[49] In order to elucidate the role of the shelf control mechanism for maintaining deep AO primary production, we conducted a numerical experiment where near-bottom remineralization of nutrients was switched off. This reduction in nutrients led to a 20% decrease of the total AO primary production, with the main impact in the deep basin of the Beaufort, Chukchi, East Siberian, and Laptev sectors where production is decreased by a factor of two. After 5 years, the impact became close to its saturation level, and further reduction of primary production did not occur. This saturation timescale was probably set by the time required for the ecosystem to utilize shelf nutrients as they were being advected into the central basin. Such a saturation timescale would also explain why there was no impact on the productivity in the deep AO adjacent to the Canadian Archipelago

and Greenland, as these areas are too far downstream from the shelf sources of nutrients.

[50] The design of our experiment did not allow us to address impacts of the interannual variability of the AO dynamical features such as accumulation of the freshwater in the surface of the Beaufort Gyre [e.g., *McLaughlin & Carmack*, 2010] and strengthening of the continental shelf pump in the Makarov Basin [*Nishino et al*., 2011).

[51] Another important, although potentially undesirable result of the shelf control experiment, is substantial decrease of the primary production over Siberian shelves. Such a decrease implies that in the model, a significant part of the shelf productivity is fuelled by the re-entrainment of nutrients remineralized at the bottom back into the upper water column. This in turn suggests that at least once during the winter, the water column is mixed down to the bottom. This is contrary to the original hypothesis of *Jones & Anderson* [1986] which instead suggests that increased near-bottom nutrients are prevented from in situ re-entrainment into the photic zone due to the strong saline stratification of the shelves and are instead advected horizontally into the deep basin. A study of *Dmitrenko et al*. [2005] based on hydrological data collected on the shelf of the Laptev Sea showed that the probability of convective mixing penetrating to the seafloor is only substantial in the region of the flaw polynya (a polynya between pack ice and land-fast ice) and may reach about 20% in the some areas of the Western and 70% in the Eastern parts of the inner shelf [cf. Figure 7 of *Dmitrenko et al*., 2005]. *Dmitrenko et al*. [2005] noted that the Laptev Sea polynya is the most distinct one across all the Siberian Seas, so we can speculate that in other shelf areas, this probability should be substantially lower. As the model, as well as most of the present-day OGCMs, does not have a dedicated land-fast model, it exaggerates the shoreward extent of the polynya, thus overestimating mixing in the shallow parts of the Siberian shelf [see e.g., *Johnson et al*., 2012 for discussion on the effects of land-fast ice). *Nguyen et al*. [2009] pointed out that salt plumes forming during the sea-ice formation and subsequent brine rejection in leads occurs at horizontal scales of 100–3000 m, a much finer scale than that typically resolved in models. When the rejected salt is spread through the much larger model grid cells, unrealistic large-scale convection occurs. *Nguyen et al*. [2009] developed a brine rejection scheme for redistributing rejected salt to the depth of its neutral buoyancy, and this showed substantial improvement in the modeled AO halocline properties.

[52] Aforementioned observational and modeling evidence suggests that by overestimating vertical mixing on the shelves, our model results may underestimate the importance of the shelf control mechanism. We can speculate that if vertical mixing on the Siberian shelf in the model is less widespread, then near-bottom increase of nutrients and their subsequent advective supply might be even more substantial. On the other hand, using recent observation of nutrients in the Makarov Basin, *Nishino et al*. [2011] argued that nutrient-rich water in this area appeared to be supplied from the shelf of the East Siberian Sea. They proposed formation of shelf bottom water through cooling followed by northward advection with high nutrient concentrations resulting from near-bottom remineralization. Further, *Nishino et al*. [2011] suggested that the formation of such water masses has become more likely in the recent years as a result of the decrease in the sea-ice cover and the delay of winter freeze-up. The significance of shelf bottom water formation suggests that the parameterization of such shelf processes is of considerable importance for basin-scale (and global) modeling studies focusing on the AO ecosystems and for the carbon cycle.

[53] The modeling study of *Slagstad et al*. [2011] suggests that primary production will increase on most shelves and Eurasian shelf break under future climate change. If such an increase occurs, it will also strengthen the supply (and subsequent remineralization) of the organic matter to the bottom layer of the broad continental shelf and its subsequent advection into the central AO, although denitrification on the shelves [e.g., *Devol et al*., 1997] may counterbalance this effect. However, the advective impact on AO ecosystems is not restricted to the nutrient supply. Its role in the distribution of biological actors has been shown in a number of studies, such as advection of a Pacific haplotype of the zooplankton *Calanus glacialis* into the AO [*Nelson et al*., 2009], link between the AO circulation pattern and variability of zooplankton *Kosobokova and Hirche* [2009] and impact of the ice reduction on the invasion of species *Reid et al*. [2008].

[54] Above mentioned studies reinforce the view of interconnectivity of the AO [e.g., *McLaughlin et al*., 2002; *Carmack & McLaughlin*, 2011]. Such interconnectivity points towards the fact that continuous retreat of the sea ice would affect AO ecosystem not only by altering in situ conditions such as light regime and stratification but also by modification of the physical and biological regimes of the remote upstream areas [*Carmack et al*., 2012].

5. Summary

[55] AO is an area where the vertical supply of nutrients is restricted due to very stable stratification and where advective processes play a major role in delivering nutrients to the photic zone. In order to investigate source and timescales of the nutrient advection, we performed a Lagrangian analysis of the mechanisms of nutrient supply to the subsurface (60–65 m) layers of the AO ecosystem. Lagrangian experiments were made on the basis of a global general circulation model coupled to an ocean ecosystem model and Lagrangian particle tracking approach.

[56] We estimated the time required by water parcels to reach subsurface waters from the three points of entry to the AO (the Bering Strait, the Barents Sea opening, and the eastern Fram Strait). Our model experiments showed that advective supply timescales in the AO do not exceed 20 years with the exception of the northeastern part of the Baffin Bay which is supplied by the route: Barents Sea opening-Arctic circumpolar current-CAA-Baffin Bay, taking an order of 25–30 years. The rest of the subsurface waters in the deep AO are connected to the NA or NP on much shorter timescales. Nutrients to the Canada basin are supplied from the Bering Strait on a timescale of 5–7 years, and to the western Amundsen Basin by the transpolar drift on the timescale of 7–10 years. The Western Nansen Basin is supplied by the Fram Strait on a timescale not exceeding 5 years, while the waters arriving from the Barents Sea opening spread through the Amundsen and Makarov

Basins on a timescale of 15–20 years. These timescales are similar to the experimental estimates of [*Ekwurzel et al*., 2001; *Karcher et al*., 2012; *Mauldin et al*., 2010; *Newton et al*., 2008; *Smith et al*., 2011].

[57] Horizontal advection of nutrient-rich shelf bottom waters is an important and fast advective route that supports an estimated 20% of total AO primary production in our simulations. Regionally, the mechanism can be much more substantial and can support up to 50–60% in the eastern Makarov and Amundsen Basins and central Canada Basin. However, not all the Arctic shelves contribute to the supply of subsurface waters. Bottom waters of the Barents and outer Kara Seas are too dense and propagate to the deep AO well below the photic zone. The Beaufort Sea shelf is too narrow to provide a substantial influence on the productivity of the deep AO. Thus, the main contributors to the supply of nutrients to the AO subsurface Chl-a maximum are the shelves of the East Siberian, Bering, and Laptev Seas.

[58] Our study draws attention to the importance of the adequate modeling of the circulation in general and the formation of nutrient-rich shelf bottom waters in particular for a realistic representation of the functioning of the AO ecosystem. Two main physical processes contributing to the shelf pump are in need of improvement in GCMs applied to the study of AO biogeochemistry: brine release mechanisms and vertical mixing on the shelf seas. Our study cautions against the one dimensional view of ecosystem dynamics in the AO and reinforces the view that Arctic ecosystems cannot be understood in regional isolation [e.g., *McLaughlin et al*., 2002; *Carmack & McLaughlin*, 2011].

Appendix A: Impact of the Frequency of Velocity Sampling on the Advective Timescale Estimates

[59] In this study, the calculation of Lagrangian trajectories was performed off-line using stored velocity field from an ocean GCM. Such off-line studies are increasingly used for analysis of the ocean circulation including in biological context of studying interrelationship between basins [see e.g., *Doos et al*., 2011, for a review of applications). The main attraction of this approach for biogeochemical applications is its off-line nature, since this permits any number of computationally inexpensive experiments based on a single computationally prohibitive physical model simulation. Additionally, and unlike experiments taking place on-line in forward simulations, it allows backwards analysis of trajectory history from destination to origin.

[60] However, the question of how frequently the velocity field must be sampled for Lagrangian calculations remains an open one that largely depends on the nature of the problem investigated, model spatial resolution, timescales of interest, and the structure of the ocean flow. As such, one would not expect a universally applicable answer to the appropriate frequency questions and certain sensitivity tests might be in order for different classes of problems. For example, *Da Costa and Blanke* [2004] performed a sensitivity study of the Lagrangian trajectories with the frequency of the input velocity field varying from 15 h to 360 days using an ocean GCM with a spatial resolution of ~200 km. The study showed that increasing the temporal frequency of the velocity field from the 30 day average (which was routinely available) to a 2.5 day average (which represented high frequency) could decrease the horizontal displacement error of trajectories for the multiannual timescales commonly used in climate studies. However, with higher-resolution global models that are run for decadal to centennial timescales, especially those with numerous biological tracers, storing data at temporal frequencies better than monthly is rarely practical. It is for this reason that 30 day averages of velocity were used in our study.

[61] However, to evaluate how our calculated advective routes and timescales were affected by the sampling frequency of modeled velocity, we repeated calculations for two velocity fields: one using 30 day averages (= our default analysis), and one using 5 day averages. For both cases, output from a single model year (= year 2000) was cycled to produce a 30 year time series of trajectories. As lower temporal frequency forcing may be anticipated to manifest as more diffuse or sluggish currents, Figure 10 illustrates January forcing currents at 30 m depth for 5 day (top; 10–15 January) and 30 day (middle; 1–30 January) forcing. While the 30 day forcing has a slightly weaker Arctic Circumpolar Boundary Current and there are some locations where the 30 day forcing exhibits less small-scale variability (e.g., the Barents Sea), the spatial pattern and magnitude of the current speeds across the AO are generally very similar.

[62] Over the timescales of the advective routes described in this study (5–30 years), deviations in the details of individual trajectories that start at the same location in these two runs can be substantial. However, as this study is more interested in the broader features shown in Figures 5 and 7, Table A1 lists the calculated means and standard deviations for the timescales for each of the entry sections shown on Figure 1 for both runs. Higher-frequency, 5 day forcing may be expected to result in advective timescales that are shorter than that for 30 day forcing. However, timescales for the three entry sections show no systematic patterns in terms of means or standard deviations. Furthermore, the root-mean-square-difference in advective timescales for the two sensitivity runs (cf. Figure 5) is 0.45 years, relative to an average advective timescale of 10.3 years over the entire ensemble. As such, there is no indication that using 5 day velocity field provides consistently faster advective timescales.

[63] Nonetheless, some differences in the spatial extent of the areas filled by the trajectories entering the AO from the three gateways were found, particularly in the East Siberian sector. In the run based on the 30 day averaged velocities, the eastern part of this sector is filled from the Bering Strait, while it is filled from the Barents Sea opening in the run based on 5 day averaged velocities. However, the rest of the deviations in the advective routes between the two runs is restricted to individual trajectories and does not exceed 10%.

[64] Given the preceding results, we can speculate that even higher-frequency timescales (~1 day) associated with, for example, the nonlinear effects of storms, may affect this conclusion and may warrant a further investigation. However, the spatial resolution of our model in the central AO (10–15 km) and the resolution of ECMWF atmospheric forcing ($1.125° \times 1.125°$ grid; e.g., *Brodeau et al*., 2010] then become insufficient to adequately address this issue as spatial scales of order of 1 km need to be resolved. These scales are currently beyond the computational resources required for global and

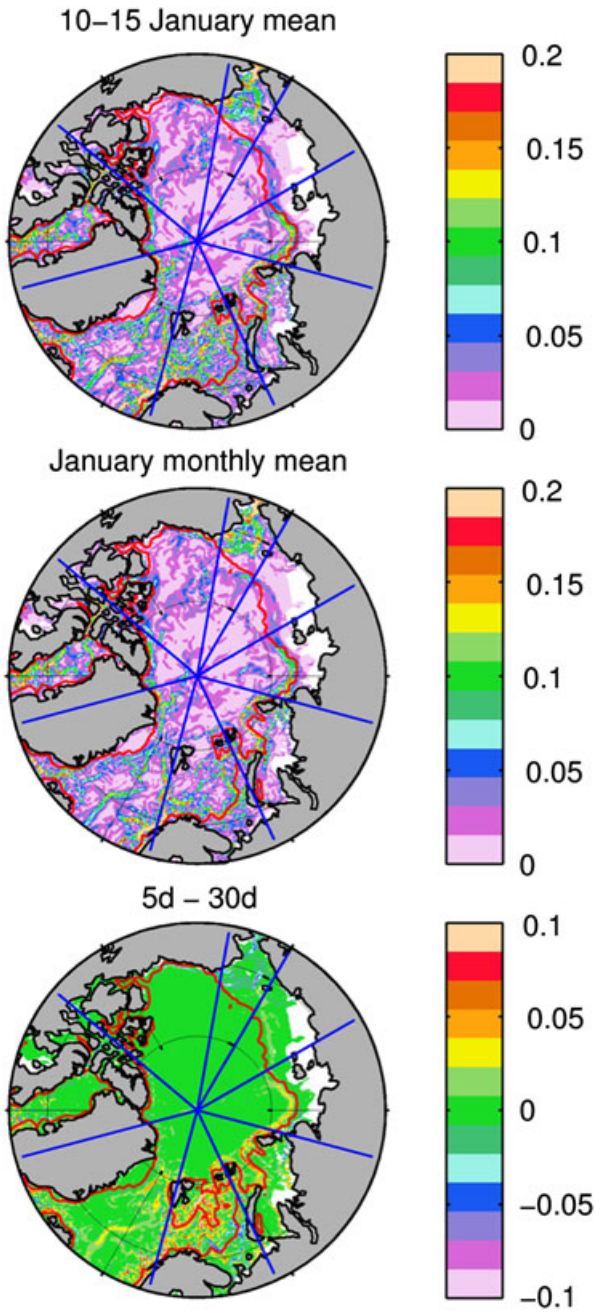

Figure 10. Currents speed (m/s) at 30 m depth for 5 day (top; 10–15 January) and 30 day (middle; 1–30 January) forcing. The bottom plot shows difference (m/s) between 5 day and 30 day averaged values.

Table A1. Mean and Standard Deviation (Years) of the Advective Timescales Calculated for the Three Entry Sections for the Runs Using 30 Day and 5 Day Mean Velocity Fields

Run	Bering Strait		Fram Strait		Barents Sea Opening	
	mean	STD	mean	STD	Mean s	STD
30 d	8.5	6.2	3.2	4.1	8.7	6.7
5 d	6.0	4.5	4.9	6.2	10.5	7.9

even pan-Arctic models. In addition, the focus of the present analysis is on trajectories that are—in the majority—at depths below 65 m. This is deeper than the maximum mixed layer depth in the Arctic [~50 m; e.g., *Rudels*, 1996], and therefore, wind mixing and high-frequency wind events, like storms, do not significantly affect these trajectories. Exceptions are the Alaskan Beaufort Sea and the Chukchi Sea, where the storm events can cause upwelling next to the shelf slope and produce a response in the ocean circulation of the halocline. However, this effect is limited to the summer and autumn months, as the presence of sea ice largely limits the magnitude of upwelling [e.g., *Pickart et al.*, 2009; *Schulze and Pickart*, 2012].

[65] Overall, we judge that the results of these two sensitivity simulations are sufficiently close for the purpose of this study, namely determining the general features of advective impacts on ocean ecosystems (with a caveat of possible errors in the East Siberian sector). However, we would still caution that similar studies, particularly those with either a more regional focus or more quantitative flux estimates, may need to use velocity fields sampled at frequency higher than monthly to minimize artifacts or errors introduced by temporal averaging.

[66] **Acknowledgments.** This study was supported by the Natural Environment Research Council, UK, as part of the National capability and UK Ocean Acidification program. We acknowledge the use of the UK National High Performance Computing Resource. This study was carried out using computational tool Ariane developed by B. Blanke and N. Grima. We are grateful to J. Blundell for help with computational aspects of Ariane.

References

Aagaard, K., L. K. Coachman, and E. Carmack (1981), On the halocline of the arctic ocean, *Deep-Sea Res. Part A-Oceanogr. Res. Pap.*, *28*(6), 529–545, doi:10.1016/0198-0149(81)90115-1.

Aagaard, K., J. H. Swift, and E. C. Carmack (1985), Thermohaline circulation in the Arctic Mediterranean Seas, *J. Geophys. Res. Oceans*, *90*(NC3), 4833–4846, doi:10.1029/JC090iC03p04833.

Aksenov, Y., S. Bacon, A. C. Coward, and N. P. Holliday (2010a), Polar outflow from the Arctic Ocean: A high resolution model study, *J. Mar. Syst.*, *83*(1–2), 14–37, doi:10.1016/j.jmarsys.2010.06.007.

Aksenov, Y., S. Bacon, A. C. Coward, and A. J. G. Nurser (2010b), The North Atlantic inflow to the Arctic Ocean: High-resolution model study, *J. Mar. Syst.*, *79*(1–2), 1–22, doi:10.1016/j.jmarsys.2009.05.003.

Aksenov, Y., V. V. Ivanov, A. J. G. Nurser, S. Bacon, I. V. Polyakov, A. C. Coward, A. C. Naveira-Garabato, and A. Beszczynska-Moeller (2011), The Arctic circumpolar boundary current, *J. Geophys. Res. Oceans*, *116*, doi:C09017 10.1029/2010jc006637.

Alkire, M. B., K. K. Falkner, I. Rigor, M. Steele, and J. Morison (2007),The return of Pacific Waters to the upper layers of the central Arctic Ocean, *Deep Sea Res. Part I*, *54*(9), 1509–1529, doi:10.1016/j.dsr.2007.06.004.

Alkire, M. B., K. K. Falkner, J. Morison, R. W. Collier, C. K. Guay, R. A. Desiderio, I. G. Rigor, and M. McPhee (2010), Sensor-based profiles of the NO parameter in the central Arctic and southern Canada Basin: New insights regarding the cold halocline, *Deep-Sea Res. Part I-Oceanogr. Res. Pap.*, *57*(11), 1432–1443, doi:10.1016/j.dsr.2010.07.011.

Anderson, L. G., T. Tanhua, G. Bjork, S. Hjalmarsson, E. P. Jones, S. Jutterstrom, B. Rudels, J. H. Swift, and I. Wahlstom (2010), Arctic ocean shelf-basin interaction: An active continental shelf CO2 pump and its impact on the degree of calcium carbonate solubility, *Deep-Sea Res. Part I-Oceanogr. Res. Pap.*, *57*(7), 869–879, doi:10.1016/j.dsr.2010.03.012.

Arrigo, K. R., G. van Dijken, and S. Pabi (2008), Impact of a shrinking Arctic ice cover on marine primary production, *Geophys. Res. Lett.*, *35*(19), doi:10.1029/2008gl035028.

Arrigo, K. R., P. A. Matrai, and G. L. van Dijken (2011), Primary productivity in the Arctic Ocean: Impacts of complex optical properties and subsurface chlorophyll maxima on large-scale estimates, *J. Geophys. Res. Oceans*, *116*, doi: 10.1029/2011jc007273.

Arthun, M., R. B. Ingvaldsen, L. H. Smedsrud, and C. Schrum (2011), Dense water formation and circulation in the Barents Sea, *Deep-Sea Res. Part I-Oceanogr. Res. Pap.*, *58*(8), 801–817, doi:10.1016/j.dsr.2011.06.001.

Beszczynska-Moeller, A., R. A. Woodgate, C. Lee, H. Melling, and M. Karcher (2011), A synthesis of exchanges through the main oceanic gateways to the Arctic Ocean, *Oceanogr.*, *24*(3), 82–99.

Blanke, B., and S. Raynaud (1997), Kinematics of the Pacific Equatorial Undercurrent: An Eulerian and Lagrangian approach from GCM results, *J. Phys. Oceanogr.*, *27*(6), 1038–1053, doi:10.1175/1520-0485(1997).

Blanke, B., M. Arhan, G. Madec, and S. Roche (1999), Warm water paths in the equatorial Atlantic as diagnosed with a general circulation model, *J. Phys. Oceanogr.*, *29*(11), 2753–2768, doi:10.1175/1520-0485(1999).

Blanke, B., S. Speich, G. Madec, and K. Doos (2001), A global diagnostic of interocean mass transfers, *J. Phys. Oceanogr.*, *31*(6), 1623–1632, doi:10.1175/1520-0485(2001).

Brodeau, L., B. Barnier A.-M. Treguier, T. Penduff, and S. Gulev (2010), An ERA40-based atmospheric forcing for global ocean circulation models, *Ocean Modelling*, *31*, 88–104, doi:10.1016/j.ocemod.2009.10.005.

Carmack, E., D. Barber, J. Christensen, R. Macdonald, B. Rudels, and E. Sakshaug (2006), Climate variability and physical forcing of the food webs and the carbon budget on panarctic shelves, *Prog. Oceanogr.*, *71* (2–4), 145–181, doi:10.1016/j.pocean.2006.10.005.

Carmack, E., and F. McLaughlin (2011), Towards recognition of physical and geochemical change in Subarctic and Arctic Seas, *Prog. Oceanogr.*, *90*(1–4), 90–104, doi:10.1016/j.pocean.2011.02.007.

Carmack, E., and P. Wassmann (2006), Food webs and physical-biological coupling on pan-Arctic shelves: Unifying concepts and comprehensive perspectives, *Prog. Oceanogr.*, *71*(2–4), 446–477, doi:10.1016/j.pocean.2006.10.004.

Carmack, E., F. McLaughlin, G. Whiteman, and T. Homer-Dixon (2012), Detecting and coping with disruptive shocks in Arctic marine systems: A resilience approach to place and people, *Ambio*, *41*(1), doi:10.1007/s13280-011-0225-6.

Cavalieri, D., C. Parkinson, P. Gloersen, and H. J. Zwally (1996), updated yearly. Sea ice concentrations from Nimbus-7 SMMR and DMSP SSM/I-SSMIS Passive Microwave Data, Sea ice concentrations. Boulder, Colorado USA: National Snow and Ice Data Center. Digital media.

Clement Kinney, J., W. Maslowski, Y. Aksenov, B. A. de Cuevas, J. Jakacki, A. Nguyen, R. Osinski, M. Steele, R. A. Woodgate, and J. Zhang, (2012), On the flow through Bering Strait: A synthesis of model results and observations, in The Pacific-Arctic Region, edited by J. Grebmeier, Springer, in press.

Curry, B., C. M. Lee, and B. Petrie (2011), Volume, freshwater, and heat fluxes through Davis Strait, 2004–05, *J. Phys. Oceanogr.*, *41*(3), 429–436, doi:10.1175/2010jpo4536.1.

Da Costa, M. V., and B. Blanke (2004), Lagrangian methods for flow climatologies and trajectory error assessment, *Ocean Modell.*, *6*(3–4), doi:10.1016/s1463-5003(03)00023-4.

Devol, A. H., L. A. Codispoti, and J.P. Christensen (1997), Summer and winter denitrification rates in western Arctic shelf sediments. *Cont. Shelf Res.*, *17*, 1029–1050.

Dmitrenko, I. A., V. V. Ivanov, S. A. Kirillov, E. L. Vinogradova, S. Torres-Valdes, and D. Bauch (2011), Properties of the Atlantic derived halocline waters over the Laptev Sea continental margin: Evidence from 2002 to 2009, *J. Geophys. Res. Oceans*, *116*, doi:10.1029/2011jc007269.

Dmitrenko, I. A., K. N. Tyshko, S. A. Kirillov, H. Eicken, J. A. Holemann, and H. Kassens (2005), Impact of flaw polynyas on the hydrography of the Laptev Sea, *Global Planet. Change*, *48*(1–3), 9–27, doi:10.1016/j.gloplacha.2004.12.016.

Doos, K. (1995), Interocean exchange of water masses, *J. Geophys. Res. Oceans*, *100*(C7), 13499–13514, doi:10.1029/95jc00337.

Doos, K., V. Rupolo, and L. Brodeau (2011), Dispersion of surface drifters and model-simulated trajectories, *Ocean Modell.*, *39*(3–4), doi:10.1016/j.ocemod.2011.05.005.

DRAKKAR Group (2007), Eddy-permitting ocean circulation hindcasts of past decades, *CLIVAR Exchanges No 42*, *12*(3), 8–10.

Ekwurzel, B., P. Schlosser, R. A. Mortlock, R. G. Fairbanks, and J. H. Swift (2001), River runoff, sea ice meltwater, and Pacific water distribution and mean residence times in the Arctic Ocean, *J. Geophys. Res. Oceans*, *106* (C5), 9075–9092, doi:10.1029/1999jc000024.

Fieg, K., R. Gerdes, E. Fahrbach, A. Beszczynska-Moeller, and U. Schauer (2010), Simulation of oceanic volume transports through Fram Strait 1995–2005, *Ocean Dyn.*, *60*(3), 491–502, doi:10.1007/s10236-010-0263-9.

Fichefet, T., Morales Maqueda, M. A. (1997), Sensitivity of a global sea ice model to the treatment of ice thermodynamics and dynamics. *J. Geophys. Res.*, *102*, 12609–12646.

Gammelsrod, T., O. Leikvin, V. Lien, W. P. Budgell, H. Loeng, and W. Maslowski (2009), Mass and heat transports in the NE Barents Sea: Observations and models, *J. Mar. Syst.*, *75*(1–2), 56–69, doi:10.1016/j.jmarsys.2008.07.010.

Garcia, H. E., R. A. Locarnini, T. P. Boyer, and J. I. Antonov, (2006). World Ocean Atlas 2005, Volume 4: Nutrients (phosphate, nitrate, silicate), edited by S. Levitus, NOAA Atlas NESDIS 64, U.S. Government Printing Office, Washington, D.C., 396 pp.

Grist, J. P., S. A. Josey, R. Marsh, S. A. Good, A. C. Coward, B. A. de Cuevas, S. G. Alderson, A. L. New, and G. Madec (2010), The roles of surface heat flux and ocean heat transport convergence in determining Atlantic Ocean temperature variability, *Ocean Dyn.*, *60*(4), 771–790, doi:10.1007/s10236-010-0292-4.

Hill, V., and G. Cota (2005), Spatial patterns of primary production on the shelf, slope and basin of the Western Arctic in 2002, *Deep-Sea Res. Part Ii-Topical Stud. Oceanogr.*, *52*(24–26), 3344–3354, doi:10.1016/j.dsr2.2005.10.001.

Johnson M., et al. (2012), Evaluation of Arctic sea ice thickness simulated by Arctic Ocean Model Intercomparison Project models, *J. Geophys. Res. Oceans*, *31*, 117, doi:10.1029/2011jc007257.

Jones, E. P., and L. G. Anderson (1986), On the origin of the chemical-properties of the Arctic-Ocean halocline, *J. Geophys. Res. Oceans*, *91* (C9), 759–767, doi:10.1029/JC091iC09p10759.

Jones, E. P., L. G. Anderson, and J. H. Swift (1998), Distribution of Atlantic and Pacific waters in the upper Arctic Ocean: Implications for circulation, *Geophys. Res. Lett.*, *25*(6), 765–768, doi:10.1029/98gl00464.

Jones, E. P., J. H. Swift, L. G. Anderson, M. Lipizer, G. Civitarese, K. K. Falkner, G. Kattner, and F. McLaughlin (2003), Tracing Pacific water in the North Atlantic Ocean, *J. Geophys. Res. Oceans*, *108*(C4), doi:10.1029/2001jc001141.

Karcher, M. J., J. N. Smith, F. Kauker, R. Gerdes, and W. M. Smethie Jr (2012), Recent changes of Arctic Ocean circulation revealed by 129 Iodine observations and modelling, *J. Geophys. Res.*, *117*, doi:10.1029/2011JC007513, in press.

Kirillov, S. A., I. A. Dmitrenko, V. V. Ivanov, E. O. Aksenov, M. S. Makhotin, and B. A. de Quevas (2012), The influence of atmospheric circulation on the dynamics of the intermediate water layer in the eastern part of the St. Anna Trough, *Dok. Earth Sci.*, *444*(1), 630–633, doi:10.1134/s1028334x12050121.

Koch-Larrouy, A., G. Madec, B. Blanke, and R. Molcard (2008), Water mass transformation along the Indonesian throughflow in an OGCM, *Ocean Dyn.*, *58*(3–4), 289–309, doi:10.1007/s10236-008-0155-4.

Kosobokova, K., and H.-J. Hirche (2009), Biomass of zooplankton in the eastern Arctic Ocean - A base line study, *Progress in Oceanography*, *82*(4), 265–280, doi:10.1016/j.pocean.2009.07.006.

Large, W. G., and S. G. Yeager (2004), Diurnal to decadal global forcing for ocean and sea-ice models: The data sets and flux climatologies, Technical Report TN-460+STR, NCAR, 105 pp.

Lique, C., A. M. Treguier, B. Blanke, and N. Grima (2010), On the origins of water masses exported along both sides of Greenland: A Lagrangian model analysis, *J. Geophys. Res. Oceans*, *115*, doi:10.1029/2009jc005316.

Madec, G. (2008), NEMO reference manual, ocean dynamic component: NEMO-OPA. Rep. 27, Note du ple de modlisation, Institut Pierre Simmon Laplace (IPSL), France, ISSN No. 1288–1619.

Marsh, R., D. Desbruyeres, J. L. Bamber, B. A. de Cuevas, A. C. Coward, and Y. Aksenov (2010), Short-term impacts of enhanced Greenland freshwater fluxes in an eddy-permitting ocean model, *Ocean Sci.*, *6*(3), 749–760, doi:10.5194/os-6-749-2010.

Martin, J., J. E. Tremblay, J. Gagnon, G. Tremblay, A. Lapoussiere, C. Jose, M. Poulin, M. Gosselin, Y. Gratton, and C. Michel (2010), Prevalence, structure and properties of subsurface chlorophyll maxima in Canadian Arctic waters, *Mar. Ecol. Prog. Ser.*, *412*, 69–84, doi:10.3354/meps08666.

Mauldin, A., P. Schlosser, R. Newton, W. M. Smethie, Jr., R. Bayer, M. Rhein, and E. P. Jones (2010), The velocity and mixing time scale of the Arctic Ocean Boundary Current estimated with transient tracers, *J. Geophys. Res. Oceans*, *115*, doi:10.1029/2009jc005965.

McLaughlin, F., E. Carmack, R. Macdonald, A. J. Weaver, and J. Smith (2002), The Canada Basin, 1989–1995: Upstream events and far-field effects of the Barents Sea, *J. Geophys. Res. Oceans*, *107*(C7), doi:10.1029/2001jc000904.

McLaughlin, F. A., and E. C. Carmack (2010), Deepening of the nutricline and chlorophyll maximum in the Canada Basin interior, 2003–2009, *Geophys. Res. Lett.*, *37*, doi:10.1029/2010gl045459.

McLaughlin, F. A., E. C. Carmack, R. W. Macdonald, and J. K. B. Bishop (1996), Physical and geochemical properties across the Atlantic Pacific water mass front in the southern Canadian Basin, *J. Geophys. Res. Oceans*, *101*(C1), 1183–1197, doi:10.1029/95jc02634.

Nelson, R. J., E. C. Carmack, F. A. McLaughlin, and G. A. Cooper (2009), Penetration of Pacific zooplankton into the western Arctic Ocean tracked with molecular population genetics, *Mar. Ecol. Prog. Ser.*, *381*, 129–138, doi:10.3354/meps07940.

Newton, R., P. Schlosser, D. G. Martinson, and W. Maslowski (2008), Freshwater distribution in the Arctic Ocean: Simulation with a high-resolution model and model-data comparison, *J. Geophys. Res. Oceans*, *113*(C5), doi:10.1029/2007jc004111.

Nguyen, A. T., D. Menemenlis, and R. Kwok (2009), Improved modeling of the Arctic halocline with a subgrid-scale brine rejection parameterization, *J. Geophys. Res. Oceans*, *114*, doi:10.1029/2008jc005121.

Nishino, S., T. Kikuchi, M. Yamamoto-Kawai, Y. Kawaguchi, T. Hirawake, and M. Itoh (2011), Enhancement/reduction of biological pump depends on ocean circulation in the sea-ice reduction regions of the Arctic Ocean, *J. Oceanogr.*, *67*(3), 305–314, doi:10.1007/s10872-011-0030-7.

Nitishinsky, M., L. G. Anderson, and J. A. Hoelemann (2007), Inorganic carbon and nutrient fluxes on the Arctic Shelf, *Cont. Shelf Res.*, *27*(10–11), 1584–1599, doi:10.1016/j.csr.2007.01.019.

Pabi, S., G. L. van Dijken, and K. R. Arrigo (2008), Primary production in the Arctic Ocean, 1998–2006, *J. Geophys. Res. Oceans*, *113*(C8), doi:10.1029/2007jc004578.

Palter, J. B., M. S. Lozier, and R. T. Barber (2005), The effect of advection on the nutrient reservoir in the North Atlantic subtropical gyre, *Nature*, *437*(7059), 687–692, doi:10.1038/nature03969.

Pickart, R. S., G. W. K. Moore, D. J. Torres, P. S. Fratantoni, R. A. Goldsmith, and J. Yang (2009), Upwelling on the continental slope of the Alaskan Beaufort Sea: Storms, ice, and oceanographic response, *J. Geophys. Res.*, *114*, C00A13, doi:10.1029/2008JC005009.

Popova, E. E., A. Yool, A. C. Coward, Y. K. Aksenov, S. G. Alderson, B. A. de Cuevas, and T. R. Anderson (2010), Control of primary production in the Arctic by nutrients and light: Insights from a high resolution ocean general circulation model, *Biogeosci.*, *7*(11), 3569–3591, doi:10.5194/bg-7-3569-2010.

Popova, E. E., A. Yool, A. C. Coward, F. Dupont, C. Deal, S. Elliott, E. Hunke, M. Jin, M. Steele, and J. Zhang (2012), What controls primary production in the Arctic Ocean?Results from an intercomparison of five general circulation models with biogeochemistry, *J. Geophys. Res. Oceans*, *117*, doi:10.1029/2011jc007112.

Proshutinsky, A., et al. (2011), Recent advances in Arctic Ocean studies employing models from the Arctic Ocean Model Intercomparison Project, *Oceanogr.*, *24*(3), 102–113.

Proshutinsky, A. Y., and M. Johnson (2001), Two regimes of the Arctic's circulation from ocean models with ice and contaminants, *Mar. Pollut. Bull.*, *43*(1–6), 61–70, doi:10.1016/s0025-326x(00)00234-4.

Proshutinsky, A. Y., and M. A. Johnson (1997), Two circulation regimes of the wind driven Arctic Ocean, *J. Geophys. Res. Oceans*, *102*(C6), 12493–12514, doi:10.1029/97jc00738.

Rayner, N. A., D. E. Parker, E. B. Horton, C. K. Folland, L. V. Alexander, D. P. Rowell, E. C. Kent, and A. Kaplan (2003), Global analyses of sea surface temperature, sea ice, and night marine air temperature since the late nineteenth century, *J. Geophys. Res. Oceans*, *108*(D14), doi:10.1029/2002jd002670.

Reid, P. C., M. Edwards, and D. G. Johns (2008), Trans-arctic invasion in modern times, *Science*, *322*(5901), 528–529.

Rudels, B., L. G. Anderson, and E. P. Jones (1996), Formation and evolution of the surface mixed layer and halocline of the Arctic Ocean, *J. Geophys. Res. Oceans*, *101*(C4), 8807–8821, doi:10.1029/96jc00143.

Rudels, B., E. P. Jones, U. Schauer, and P. Eriksson (2004), Atlantic sources of the Arctic Ocean surface and halocline waters, *Polar Res.*, *23*(2), 181–208, doi:10.1111/j.1751-8369.2004.tb00007.x.

Rutgers van der Loeff, M. R., P. Cai, I. Stimac, D. Bauch, C. Hanfland, T. Roeske, and S. B. Moran (2012), Shelf-basin exchange times of Arctic surface waters estimated from Th-228/Ra-228 disequilibrium, *J. Geophys. Res. Oceans*, *117*, doi:10.1029/2011jc007478.

Sarmiento, J. L., N. Gruber, M. A. Brzezinski, and J. P. Dunne (2004), High-latitude controls of thermocline nutrients and low latitude biological productivity, *Nature*, *427*(6969), 56–60, doi:10.1038/nature02127.

Schlosser, P., R. Bayer, G. Bonisch, L. W. Cooper, B. Ekwurzel, W. J. Jenkins, S. Khatiwala, S. Pfirman, and W. M. Smethie (1999), Pathways and mean residence times of dissolved pollutants in the ocean derived from transient tracers and stable isotopes, *Sci. Total Environ.*, *238*, 15–30.

Schweiger, A., R. Lindsay, J. Zhang, M. Steele, H. Stern, and R. Kwok (2011), Uncertainty in modeled Arctic sea ice volume, *J. Geophys. Res. Oceans*, *116*, doi:10.1029/2011jc007084.

Schulze, L. M., and R. S. Pickart (2012), Seasonal variation of upwelling in the Alaskan Beaufort Sea: Impact of seaice cover, *J. Geophys. Res.*, *117*, C06022, doi:10.1029/2012JC007985.

Serreze, M. C., A. P. Barrett, A. G. Slater, R. A. Woodgate, K. Aagaard, R. B. Lammers, M. Steele, R. Moritz, M. Meredith, and C. M. Lee (2006), The large-scale freshwater cycle of the Arctic, *J. Geophys. Res. Oceans*, *111*(C11), doi:10.1029/2005jc003424.

Slagstad, D., I. H. Ellingsen, and P. Wassmann (2011), Evaluating primary and secondary production in an Arctic Ocean void of summer sea ice: An experimental simulation approach, *Prog. Oceanogr.*, *90*(1–4), 117–131, doi:10.1016/j.pocean.2011.02.009.

Smedsrud, L. H., R. Ingvaldsen, J. E. O. Nilsen, and O. Skagseth (2010), Heat in the Barents Sea: transport, storage, and surface fluxes, *Ocean Sci.*, *6*(1), 219–234.

Smith, J. N., F. A. McLaughlin, W. M. Smethie, Jr., B. Moran, and K. Lepore (2011), Iodine-129, Cs-137, and CFC-11 tracer transit time distributions in the Arctic Ocean, *J. Geophys. Res. Oceans*, *116*, doi:10.1029/2010jc006471.

Speich, S., B. Blanke, and G. Madec (2001), Warm and cold water routes of an OGCM thermohaline conveyor belt, *Geophys. Res. Lett.*, *28*(2), 311–314, doi:10.1029/2000gl011748.

Steele, M., J. Morison, W. Ermold, I. Rigor, M. Ortmeyer, and K. Shimada (2004), Circulation of summer Pacific halocline water in the Arctic Ocean, *J. Geophys. Res. Oceans*, *109*(C2), doi:10.1029/2003jc002009.

Taylor, P. D., and D. L. Feltham (2004), A model of melt pond evolution on sea ice, *J. Geophys. Res.*, *109*, C12007, doi:10.1029/2004JC002361.

Timmermann, R., H. Goosse, G. Madec, T. Fichefet, C. Ethe, and V. Duliere (2005), On the representation of high latitude processes in the ORCA-LIM global coupled sea ice-ocean model, *Ocean Modell.*, *8*(1–2), 175–201, doi:10.1016/j.ocemod.2003.12.009.

Timmermans, M.-L., A. Proshutinsky, R. A. Krishfield, D. K. Perovich, J. A. Richter-Menge, T. P. Stanton, and J. M. Toole (2011), Surface freshening in the Arctic Ocean's Eurasian Basin: An apparent consequence of recent change in the wind-driven circulation, *J. Geophys. Res.*, *116*, C00D03, doi:10.1029/2011JC006975.

Tremblay, J. E., et al. (2011), Climate forcing multiplies biological productivity in the coastal Arctic Ocean, *Geophys. Res. Lett.*, *38*, doi:10.1029/2011gl048825.

Tremblay, J. E., and J. Gagnon (2009), The effects of irradiance and nutrient supply on the productivity of Arctic waters: a perspective on climate change, *Influence of Clim. Change on the Changing Arct. Sub-Arct. Conditions*, *73–93*, doi:10.1007/978-1-4020-9460-6_7.

Tsubouchi, T., S. Bacon, A. C. N. Garabato, Y. Aksenov, S. W. Laxon, E. Fahrbach, A. Beszczynska-Moeller, E. Hansen, C. M. Lee, and R. B. Ingvaldsen (2012), The Arctic Ocean in summer: A quasi-synoptic inverse estimate of boundary fluxes and water mass transformation, *J. Geophys. Res. Oceans*, *117*, doi:10.1029/2011jc007174.

Wassmann, P. (2011), Arctic marine ecosystems in an era of rapid climate change, *Prog. Oceanogr.*, *90*(1–4), 1–17, doi:10.1016/j.pocean.2011.02.002.

Williams, W. J., and E. C. Carmack (2008), Combined effect of wind-forcing and isobath divergence on upwelling at Cape Bathurst, Beaufort Sea, *J. Mar. Res.*, *66*(5), 645–663.

Yool, A., E. E. Popova, and T. R. Anderson (2011), MEDUSA-1.0: a new intermediate complexity plankton ecosystem model for the global domain, *Geosci. Model Dev.*, *4*(2), 381–417, doi:10.5194/gmd-4-381-2011.

Zhang, J., and D. A. Rothrock (2003), Modeling global sea ice with a thickness and enthalpy distribution model in generalized curvilinear coordinates, *Mont. Weather Rev.*, *131*(5).